

1 How much do zooplankton and fine-scale processes
2 matter for the ocean biological pump?

3 Mathieu A. Poupon^{1,2*}, Laure Resplandy^{1,3} and Jessica Y. Luo⁴

4 ¹Department of Geosciences, Princeton University, Princeton, 08544,
5 NJ, USA.

6 ²Atmospheric and Oceanic Sciences Program, Princeton University,
7 Princeton, 08540, NJ, USA.

8 ³High Meadows Environmental Institute, Princeton University,
9 Princeton, 08544, NJ, USA.

10 ⁴NOAA Geophysical Fluid Dynamics Laboratory, Princeton, 08540, NJ,
11 USA.

12 *Corresponding author(s). E-mail(s): mpoupon@princeton.edu;
13 Contributing authors: laurer@princeton.edu; jessica.luo@noaa.gov ;

14 **Abstract**

15 The ocean biological carbon pump stores carbon away from the atmosphere
16 through multiple pathways, including gravitational settling, physical transport,
17 and organism vertical migration. Robust assessments of its magnitude remain
18 challenging. Traditional approaches often treat individual pathways separately,
19 risking double counting when combining estimates, fail to capture high-frequency
20 processes such as finescale physics and daily vertical migration over large scales,
21 and focus on particulate carbon while overlooking non-particulate fluxes. Here,
22 we apply a unified framework quantifying all pathways simultaneously to a
23 high-resolution (3km) idealized model of the North Atlantic resolving seasonal,
24 biophysical dynamics –including zooplankton migration – from fine-scale kilomet-
25 ric fronts to regional biomes. We show that the fine-scale physical and migrant
26 pumps collectively contribute 15–20% to carbon storage, providing effective path-
27 ways complementing the gravitational pump. Fine-scale dynamics modulate
28 carbon export depth and storage timescales, acting directly through the physical
29 pump and indirectly by shaping fast-sinking, carbon-rich filaments (gravita-
30 tional pump) and controlling zooplankton migration depths (migrant pump).
31 Remarkably, carbon storage by the physical and migrant pumps is dominated
32 by non-particulate carbon fluxes —dissolved organic carbon transport and zoo-
33 plankton respiration. Adequately measuring and representing these pathways in

34 next-generation observations and models is key to quantify ocean carbon storage
35 and its response to variability.

36 **Keywords:** Biological carbon pump, Non-particulate fluxes, Ocean carbon cycle

37 1 Introduction

38
39 The ocean's biological carbon pump is a critical engine of the climate system, storing
40 carbon away from the atmosphere [1, 2]. This carbon storage occurs through a set of
41 interconnected processes—referred to as 'pumps'—exporting and remineralizing both
42 particulate and dissolved organic carbon in the ocean interior (Fig 1a,A1) [3]. Current
43 estimates suggest these pumps export between 5 and 12 PgC yr⁻¹ from the surface
44 ocean [4–8] and store between 1100 and 1500 PgC in the ocean interior [8, 9]. However,
45 none of these estimates fully capture all the pumps and their spatial and temporal
46 scales, hindering our ability to accurately assess the biological carbon pump's current
47 magnitude, its response to climate change, and role as a climate feedback – reinforcing
48 or dampening of climate change by biological pump changes[10].

49
50 A comprehensive assessment of the biological pump requires disentangling intricate
51 processes that export both particulate and dissolved organic carbon on different time
52 and space scales. The most well-studied pump is the gravitational pump, which is
53 fueled by sinking particles (Fig 1b). The physical pumps transport both particulate
54 and dissolved carbon through three mechanisms (Fig 1c): the large-scale pump trans-
55 fers carbon via Ekman transport and overturning circulation [11], the mixed-layer
56 pump exports carbon through seasonal mixed layer deepening and restratification
57 [12, 13], and the eddy subduction pump through turbulent ocean dynamics, includ-
58 ing fine-scale eddies and fronts (< 200 km)[14, 15], a pathway that has only been
59 recently studied. Fine-scale dynamics also modulate upper-ocean stratification, nutri-
60 ent supply, primary production, and trophic interactions[15–18], thereby shaping the
61 biological carbon pump beyond carbon transport alone. Finally, the migrant pump
62 is powered by vertically migrating organisms, such as zooplankton, which actively
63 transport particulate and dissolved carbon through egestion, excretion, and respiration
64 along their migration path (Fig 1d) [19–21]. While zooplankton vertical migration
65 has been described for 200 years [22], until recently, not much has been known about
66 its contribution to the biological pump. Full assessments are challenging due to the
67 vast range of scales that these pumps span. Zooplankton migration occurs daily over
68 hours and hundreds of meters [23], climate-driven circulation changes extend over
69 decades and global scales [7, 24, 25], and in between, submesoscale fronts [14, 17] and
70 mesoscale eddies [15, 26, 27] act on spatial scales of 1–100 km and temporal scales
71 from days to months. This complexity and variability pose significant challenges for
72 existing observational and modeling tools [28].

73

74 Current evaluations remain limited by the partial characterization of the pumps and
 75 the poor resolution of seasonal and fine-scale dynamics, leading to fragmented and
 76 incomplete estimates. Observational approaches often overlook non-particulate car-
 77 bon fluxes, which are harder to measure than particulate fluxes [29–31] and tend to
 78 largely exclude suspended and ascending particles[32]. Model studies either represent
 79 zooplankton migration using simplified parameterizations[8, 20, 33] that fail to cap-
 80 ture its full complexity, or omit it due to computational and conceptual trade-offs
 81 [7, 15, 24]. Typically, studies focus on a single pump at a time [29, 34–36], without
 82 isolating the contributions of other pumps, potentially causing double counting when
 83 aggregating individual estimates [3, 37]; e.g., migrant-produced fecal pellets can be
 84 counted in both the migrant and gravitational pumps. Estimates are also constrained
 85 in spatio-temporal scales. Observations provide valuable snapshots in time and space
 86 but are challenging to extrapolate at regional and seasonal scales. Meanwhile, many
 87 global and regional models fail to resolve fine-scale processes such as eddies and fronts,
 88 playing a critical role in carbon export [15, 38]. Finally, while most studies focus on
 89 export fluxes, they rarely consider the depth at which this carbon is remineralized
 90 by bacterial breakdown or zooplankton respiration, which is key in determining the
 91 timescale over which it remains stored in the interior ocean [2].

92

93 Here, we address these challenges by quantifying how much organic carbon leaves the
 94 sunlit surface ocean (export, $\text{gC m}^{-2} \text{ yr}^{-1}$) and how much is stored in the ocean
 95 interior as dissolved inorganic carbon (storage, gC m^{-2}) by the different components
 96 of the biological carbon pump, using an idealized high-resolution model of the North
 97 Atlantic Ocean (DG-MOM6-COBALTv2-DVM[39]). This region covers contrasting
 98 biomes featuring marked seasonality and fine-scale dynamics [15, 38], and supports
 99 active gravitational, physical, and migrant carbon pumps [13, 19, 40, 41], offering a
 100 representative setting to understand their contribution to global carbon export and
 101 storage. Our model explicitly resolves these three pumps and covers their spatio-
 102 temporal dynamics from hourly and kilometric scales to seasonal and regional scales.
 103 We show that the physical and migrant pumps store more carbon via the export of
 104 non-particulate carbon (dissolved organic carbon transport, migrating zooplankton
 105 respiration) than via particle export, highlighting the need to better account for these
 106 fluxes in biological carbon pump assessments. Our results further show that fine-scale
 107 processes shape carbon export and storage directly via the eddy-subduction pump,
 108 but also by modulating the export magnitude and depth of the other pumps. We argue
 109 that adequately characterizing biophysical complexity –including fine-scale processes,
 110 biological migration and non-particulate carbon fluxes– is key to capturing current
 111 ocean carbon storage and its response to future changes.

112 2 Carbon Flux Contrasts in the North Atlantic

113

114 Our double gyre model reproduces the observed fine-scale and large-scale biophysical
115 dynamics that structure the North Atlantic biological carbon pump, including primary
116 productivity, migrating zooplankton biomass and vertical winter mixing (Fig 2, see
117 details in Poupon et al. 2025 [39]). Specifically, the model captures the variability asso-
118 ciated with turbulent dynamics, as shown by kilometric-scale chlorophyll filaments,
119 reflecting fine-scale variations in primary productivity, and by eddy kinetic energy pat-
120 terns, both matching satellite observations (Figs 2a-b, A2). The model also simulates
121 the regional contrast between the high-productivity, high-seasonality subpolar biome
122 (annual surface chlorophyll $> 0.35 \text{ mg m}^{-3}$) and low-productivity, low-seasonality
123 subtropical biome (annual surface chlorophyll $< 0.15 \text{ mg m}^{-3}$, Fig 2c-d). In the sub-
124 polar biome, primary productivity peaks between May and June ($0.92 \text{ gC m}^{-2} \text{ d}^{-1}$
125 in model and $0.65\text{-}0.93 \text{ gC m}^{-2} \text{ d}^{-1}$ in satellite, Fig 2e), followed by migrating zoo-
126 plankton biomass that peaks between May and September (1.2 g m^{-2} in model and
127 1.4 g m^{-2} in observations, Fig 2g), with both reaching their minimum in winter (0.14
128 $\text{gC m}^{-2} \text{ d}^{-1}$ and 0.7 g m^{-2} in model, $0.10\text{-}0.24 \text{ gC m}^{-2} \text{ d}^{-1}$ and 0.4 g m^{-2} in
129 satellite, Fig 2e,g). In contrast, in the subtropical biome, primary productivity and
130 zooplankton migrant biomass remain relatively low and stable year-round ($0.17\text{-}0.25$
131 $\text{gC m}^{-2} \text{ d}^{-1}$ and $0.1\text{-}0.3 \text{ g m}^{-2}$, in both model and observations, Fig 2e,g). The model
132 also captures the contrasting physical dynamics between the subpolar biome, where
133 the mixed layer depth strongly varies from shallow summer (25-35 m) to deep winter
134 (120-140 m) values, and the subtropical biome where it stays relatively shallow (30-60
135 m, Fig 2f).

136

137 These regional biophysical differences drive high carbon export and storage con-
138 trasts between subpolar and subtropical biomes. The simulated annual carbon export
139 (defined as net carbon exported and remineralized below the euphotic zone, see
140 Methods) in the high-productivity subpolar biome is 3 times greater than in the low-
141 productivity subtropical biome ($36 \text{ vs } 12 \text{ gC m}^{-2} \text{ yr}^{-1}$, Fig 3a, A3). This contrast is
142 further amplified because, for any given depth at which remineralization occurs, car-
143 bon remains stored for longer in the subpolar biome than in the subtropical biome
144 (based on storage times from the Ocean Circulation Inverse Model [8], see Fig A4 and
145 Methods). As a result, carbon storage is 3.6 times greater in the subpolar biome than
146 in the subtropical biome ($5.8 \text{ vs } 1.6 \text{ kgC m}^{-2}$, Fig 3c). Despite these differences, we
147 show in the following that relative contributions of the different pumps to export and
148 storage, and the contribution of non-particulate components are remarkably similar
149 across the two biomes.

150 3 Carbon Pump Contributions to Export and Storage

151

152 Our analysis reveals that the relative contributions of the gravitational, physical, and
153 migrant pumps to carbon export and storage are similar across the subpolar and
154 subtropical biomes (Fig. 3b). The gravitational pump dominates export (~60% in
155 both biomes), followed by the physical pumps (~30%; mixed-layer: 10–12%, large-
156 scale: 5–18%, eddy-subduction: 5–9%), and the migrant pump (~10%; subtropical:
157 6%, subpolar: 11%). Pumps contributions to storage differ from export (Fig. 3b,d).
158 The gravitational pump is highly efficient, with a contribution to storage that exceeds
159 that of export (~70% vs. ~60%). In contrast, physical pumps are less efficient and
160 contribute less to storage than to export (ranging from 17 to 25% across biomes; mixed-
161 layer: 1 to 4%, large-scale: 2 to 20%, eddy-subduction: 5 to 10%). The migrant pump
162 contributes similarly in both biomes (subtropical: 5%, subpolar: 10%, Fig. 3b,d).

163

164 These differences in pump efficiency are controlled by the depth at which organic car-
165 bon exported by each pump is remineralized in our model (Fig. 3a-d). The deeper the
166 remineralization –via bacterial breakdown of POC and DOC or zooplankton respira-
167 tion (see Methods)– the longer the carbon remains stored, and the more efficient the
168 pump (Fig. A4). Overall, most of the carbon stored by the biological pumps in the
169 model is remineralized in the mesopelagic zone in both biomes (75% in upper 1000
170 meters, 50% in upper 500 meters, Fig. 4a-d), consistent with recent findings [42]. How-
171 ever, the organic carbon exported by each pump is remineralized over distinct depth
172 ranges. In both biomes, carbon exported by the gravitational pump is remineralized
173 on average 250–280 m below euphotic zone, making this pump the most efficient (Fig.
174 4a,d). Carbon exported by physical pumps is largely remineralized at shallower depths
175 (Fig. 4b), similar to previous work[31], however our model shows large differences
176 between export pathways. The eddy-subduction pump exports carbon on average 200–
177 270 m below the euphotic zone, while the large-scale pump exports it on average
178 100–270 m below and the mixed-layer pump only 0–80 m below (Fig. 4d). Finally, the
179 carbon exported by the migrant pump is mainly remineralized 170–190 m below the
180 euphotic zone (Fig. 4c,d). Thus, the eddy subduction pump and the migrant pump
181 are highly efficient storage pathways that complement the gravitational pump.

182 4 Importance of Non-Particulate Carbon Fluxes

183

184 Fluxes of non-particulate carbon from the physical pump (DOC transport) and
185 migrant pump (injection of DIC by zooplankton respiration) support more than 20% of
186 the total simulated carbon export and storage in the subpolar and subtropical biomes
187 (Fig 3c,d). The physical transport of DOC contributes ~ 62% to the physical pump
188 storage (eddy-subduction pump: 19%, large scale pump: 39%, mixed layer pump: 4%),
189 while that of POC, including plankton and sinking detritus, only contributes ~ 38%
190 (Fig. 3d, Fig. A5). This large contribution of DOC to the physical pump storage is

controlled by the different fate of exported DOC and POC in the water column. In fact, the physical pumps export more POC than DOC from the euphotic zone (14-19% vs 12-14% of total export, Fig 3f and Fig A5), but POC is more rapidly remineralized (~hours to weeks) than DOC (labile DOC: days, semi-labile DOC: months, semi-refractory DOC: decades), allowing DOC to be transported deeper by ocean currents before decomposition (+200-300m vs +60-80m below the euphotic zone, Fig 4f,h). Specifically, remineralization of semi-refractory DOC accounts for most of the storage by the physical pump in the model (Fig A5) making it a key pathway of the biological carbon pump.

Contrary to the traditional view [3], the migrant pump stores carbon primarily through the injection of DIC via migrating zooplankton respiration. This respiratory flux accounts for 90% of the migrant pump carbon storage in our model (Fig 3d, 4g,h). In contrast, POC egested by migrating zooplankton is largely confined to the euphotic zone (upper 100m, Fig A6). This is mainly because digestion and egestion of POC by zooplankton occurs rapidly –within 15 minutes to 3 hours after feeding (Fig A7, [43]) while zooplankton are still in the upper ocean. In contrast, zooplankton continuously respire [44, 45], injecting a larger amount of DIC at their migration depth (~300-500 m, Fig 4g,h) where they spent 9-17 hours during daytime (Fig. A7), leading to longer storage times for the injected DIC than for the egested POC (Fig 4g,h). We conclude that carbon storage by the non-particulate components of the physical and migrant pumps exceeds that of their particulate counterparts, at odds with the focus of previous studies quantifying these pumps [3, 29, 30].

5 Fine-Scale Dynamics Shape Carbon Export and Remineralization Depths

Fine-scale eddies and fronts modulate both the magnitude and depth of carbon export, as illustrated by these model snapshots from March 5 (Fig. 5). Physical export shows the strongest fine-scale variability (Fig. 5b): within just a few tens of kilometers, intense export filaments ($0.1\text{--}3 \text{ gC m}^{-2} \text{ d}^{-1}$) are offset by equally strong re-entrainment into the euphotic zone ($-0.1 \text{ to } -3 \text{ gC m}^{-2} \text{ d}^{-1}$), limiting the net export. Local estimates therefore far exceed the regional net export, which cannot be meaningfully inferred without fully resolving these compensating fluxes. Gravitational export varies from 0.05 to $0.3 \text{ gC m}^{-2} \text{ d}^{-1}$ at fine scale (Fig. 5a), reflecting transitions between highly productive filaments—producing sinking particles such as aggregates and fecal pellets—and weakly productive ones (Fig. 2b). Migrant export also exhibits fine-scale variations on the order of $0.003\text{--}0.01 \text{ gC m}^{-2} \text{ d}^{-1}$, driven by the heterogeneous spatial distribution of migrating zooplankton and their prey (Fig. SA8). These patterns occur in both biomes and persist throughout the year (Fig. SA9).

230 Our analysis shows that fine-scale dynamics also modulate the carbon export depth of
231 each pump (Fig. 5d–f) and the associated carbon storage (Fig. 5g–i). Physical export
232 depth is the most variable, ranging between +20 m and +450 m below the base of
233 the euphotic layer over a few tens of kilometers (Fig. 5e), yet we do not detect a sys-
234 tematic small-scale covariation between export depth and export magnitude for the
235 physical pump (Fig. 5h). In contrast, fine-scale dynamics modulate migrant export
236 depth, from +50 m to +350 m below the euphotic zone (Fig. 5f), primarily by redis-
237 tributing chlorophyll (Fig. 2b). In highly productive filaments, chlorophyll-induced
238 shading locally reduces light levels, shoaling zooplankton migration and the depth
239 at which DIC is injected by respiration [39]. As a result, hotspots of migrant export
240 tend to coincide with shallower export depths (Fig. 5i), which limits storage. Gravi-
241 tational export depth also varies at fine scales, from about +150 m to +400 m below
242 the euphotic layer (Fig. 5d), but in this case hotspots of gravitational export tend
243 to coincide with deeper export depths (Fig. 5g), which could reflect more effective
244 particle ballasting and shielding in these filaments (Fig. A8) that allow aggregates to
245 sink farther before remineralization and thus enhance storage. Annually, these fine-
246 scale covariations reduce migrant pump storage by about $\sim 5\%$ in both biomes, while
247 increasing gravitational pump storage by about 0.5–1.5% (Fig. A12). Together, these
248 patterns show that fine-scale dynamics do not merely transport and redistribute car-
249 bon, but selectively amplify or reduce carbon storage by the different components of
250 the biological carbon pump.
251

252 **6 Bringing Biophysical Complexity into Future 253 Observational and Modeling Paradigms**

254 In both subtropical and subpolar biomes, we show that carbon storage by the migrant
255 and physical pumps is dominated by non-particulate carbon fluxes, which together
256 account for about 20% of total storage. In practice, these so-called “particle injection
257 pumps”[3] are in fact mainly non-particulate pumps: the migrant pump via respi-
258 ration and the physical pumps via the transport of DOC, suggesting a refinement
259 in how these pathways should be considered. Our results are consistent with pre-
260 vious work[8], who showed that DOC dominates the large-scale pump yearly. Here,
261 we show that this is also the case at fine scales, where the eddy-subduction pump
262 stores most of the carbon via DOC transport. We also confirm large offsets between
263 upward and downward fluxes previously reported[15]. This matters because current
264 observational studies on the eddy-subduction export mostly focus on POC and do
265 not take these limitations into account[29, 37]. Current approaches have been devel-
266 oped to estimate DOC transport from floats [46, 47], as well as upward/downward
267 sub-mesoscale transport[48], and should be leveraged to evaluate their global impact.
268 Additionally, recent progress in the understanding of microbial processes that rem-
269 ineralize organic carbon[49, 50] and alter its reactivity[51, 52] paves the way to better
270 constrain its fate in the interior ocean. Our estimates of migrant export are lower than
271 some previous work[21], that also consider higher trophic level migration. However,

273 the ecological and biogeochemical models were not coupled—an approach that tends
274 to overestimate fluxes, as past studies have shown[53, 54]. Estimates based on simple
275 parameterization embedded in biogeochemical models tend to lie much closer to our
276 results[20, 33]. A refinement of these estimates of migrating zooplankton respiration
277 should account for coupled and extended size spectra, incorporating allometric res-
278piration rates and migration depths[55], as well as physiological cyclicity associated
279 with internal circadian rhythms[56].

280

281 We show that both the eddy-subduction pump and the migrant pump sustain deep
282 carbon export and remineralization, making them efficient storage pathways comple-
283 menting the gravitational pump. For instance, both of them account for about ~10% of
284 carbon storage in the subpolar biome. We further demonstrate that fine-scale dynamics
285 regulate carbon storage, not only via the eddy-subduction pump, but also by shaping
286 the spatial patterns and covariance in export magnitude and export depth for both the
287 gravitational and migrant pumps, modulating their respective storage. Current Earth
288 system models—routinely used to assess the future evolution of the biological car-
289 bon pump [24]—do not represent these mechanisms[57]. They are primarily tuned to
290 reproduce the bulk global export flux below the euphotic zone, which they may match
291 for the wrong reasons, while misrepresenting the remineralization of this flux, the effi-
292 ciency of the different pumps, and deep-ocean carbon storage [58, 59]. For example, if
293 zooplankton do not migrate, respired carbon remains in the surface layers, and carbon
294 that could have been exported to depth by fine-scale processes is instead transported
295 only shallowly by the mixed-layer pump, reducing carbon storage [11, 55]. In addition,
296 these export pathways are driven by distinct mechanisms whose responses to future
297 climate change can be opposite in sign and remain highly uncertain [10]. Given the
298 demonstrated importance of these pathways and their interactions, we argue that they
299 must be incorporated into Earth system models[60], most likely through parameteriza-
300 tions informed by multiscale modeling and designed to respond consistently to future
301 changes in stratification, productivity, and temperature. Without this, projections of
302 future ocean carbon storage will remain systematically incomplete and uncertain.

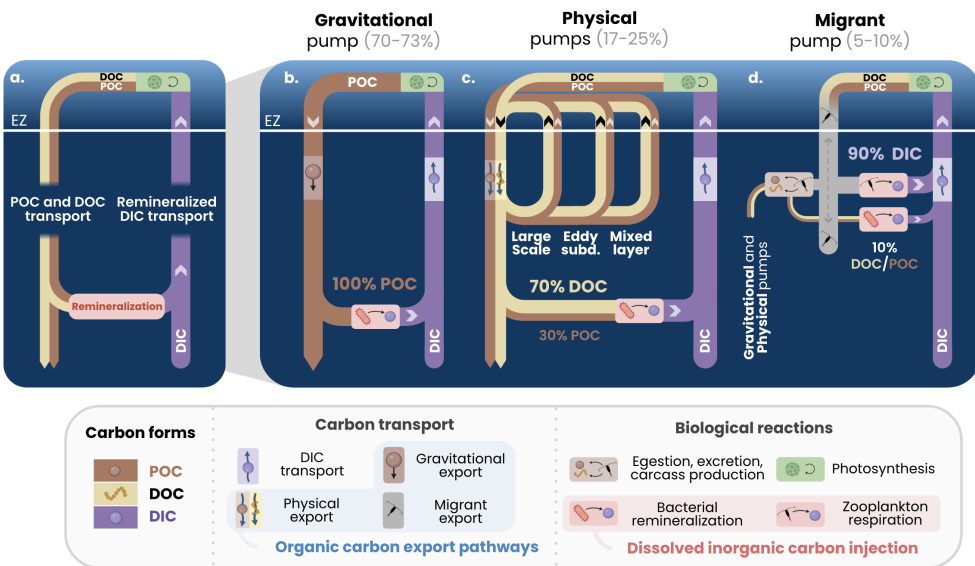


Fig. 1 Biological carbon pump as represented in COBALTv2-DVM. (a) The biological carbon pump encompasses the (b) gravitational, (c) physical and (d) migrant pumps. The physical pumps include the large-scale pump, the eddy-subduction pump and the mixed-layer pump. These pumps act to increase the vertical DIC gradient, via the production, export and remineralization of organic carbon, while the upward transport of remineralized DIC acts to decrease this gradient. Organic carbon is produced in dissolved and particulate form in the euphotic zone (EZ) through photosynthesis (green block), and is exported by the pumps. POC (brown) is transferred by gravitational settling, physical export, egestion of fecal pellets and the carcasses of migrating zooplankton. DOC (yellow) is transferred by the physical export and the excretion of migrating zooplankton. Remineralization of POC and DOC by bacteria and respiration by migrating zooplankton (red blocks) inject DIC (purple), which is stored in the interior ocean before being upwelled to the surface, closing the loop. Note that the arrow thickness is not conservative and proportional to the flux magnitudes. The schematic focuses on the component of the biological pump represented in the COBALTv2-DVM model; other pathways (e.g. dark CO₂ fixation via chemoautotrophy[61, 62]) are not included.

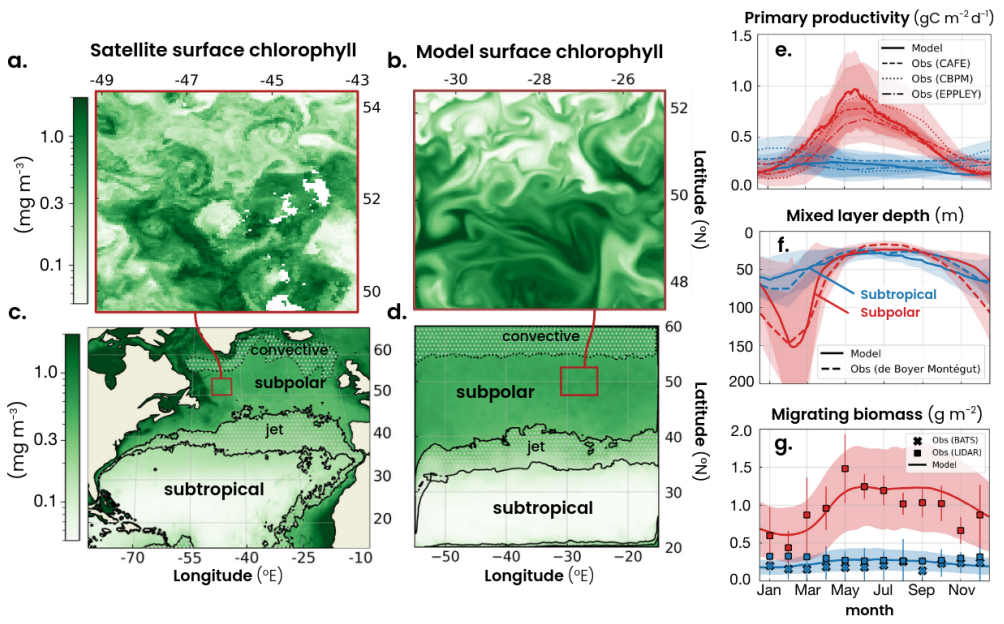


Fig. 2 Subpolar surface chlorophyll concentration snapshot from (a) satellite observations and (b) the double gyre model on March 10th. Mean annual surface chlorophyll concentration from (c) satellite observations and (d) the double gyre model. Seasonal cycle of (e) net primary productivity, (f) mixed layer depth, and (g) migrating zooplankton biomass from observations (dotted lines) and in the model (solid lines). for the subpolar (blue) and subtropical (red) biomes. Shadings show the spatial variability within each biome (two standard deviations). Subtropical and subpolar biomes are defined by annual chlorophyll concentrations lower than 0.15 mg m^{-3} and higher than 0.35 mg m^{-3} respectively (black lines in a-b). Deep convection region defined by an annual mixed layer depth $> 150 \text{ m}$, and the jet region defined by chlorophyll concentrations between $0.15\text{--}0.35 \text{ mg m}^{-3}$, are excluded from the biome analysis (dotted areas in a-b). Sources of the observations are detailed in the method section.

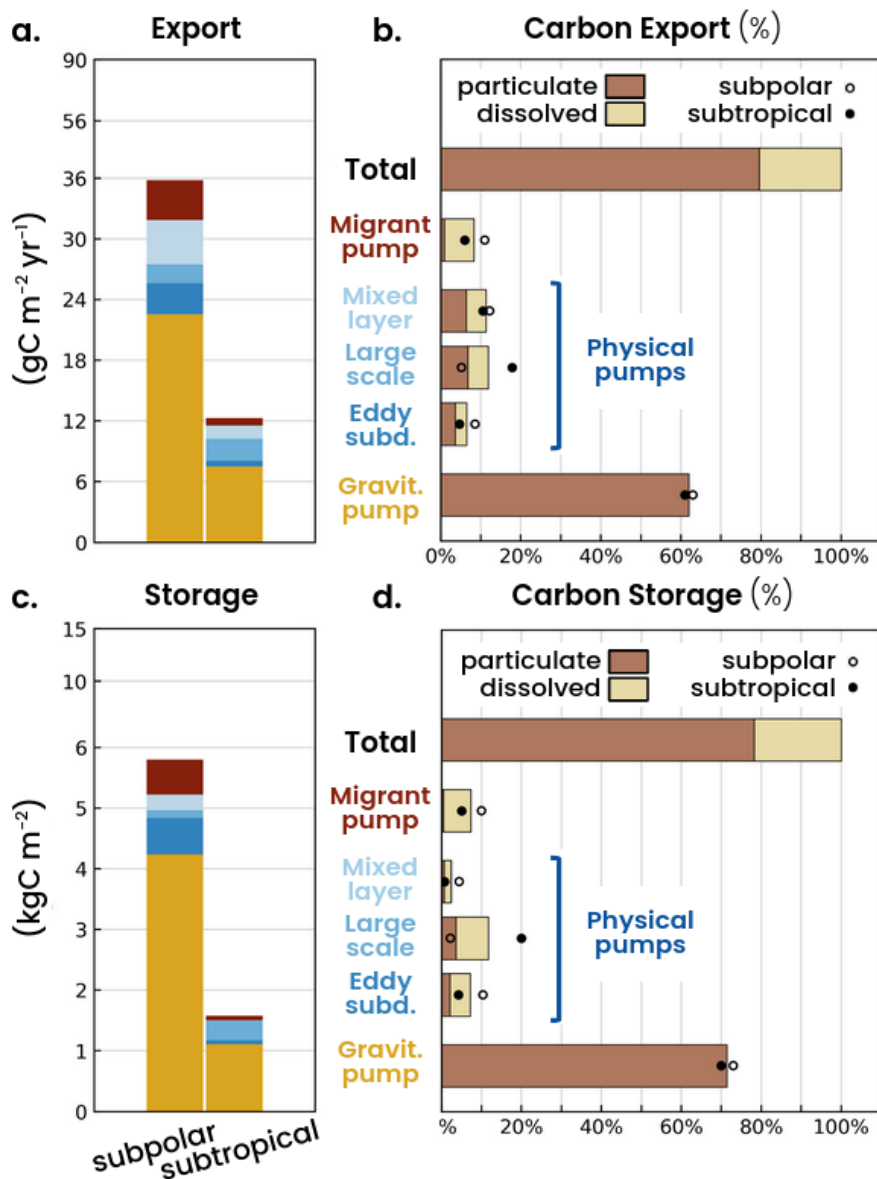


Fig. 3 (a) Annual carbon export and (c) carbon storage in the subpolar (left bars) and subtropical (right bars) biomes, partitioned among the gravitational (yellow), physical (blues), and migrant (red) pumps. The physical pumps include the mixed layer (light blue), large-scale (blue), and eddy-subduction (dark blue) pumps. (b,d) Relative contributions of each pump to (b) carbon export and (d) storage across the model domain (excluding convective region; see Methods). Pale yellow bars represent dissolved carbon fluxes, and brown bars represent particulate fluxes. Empty circles are the averages over the subpolar biome and filled circles over the subtropical biome.

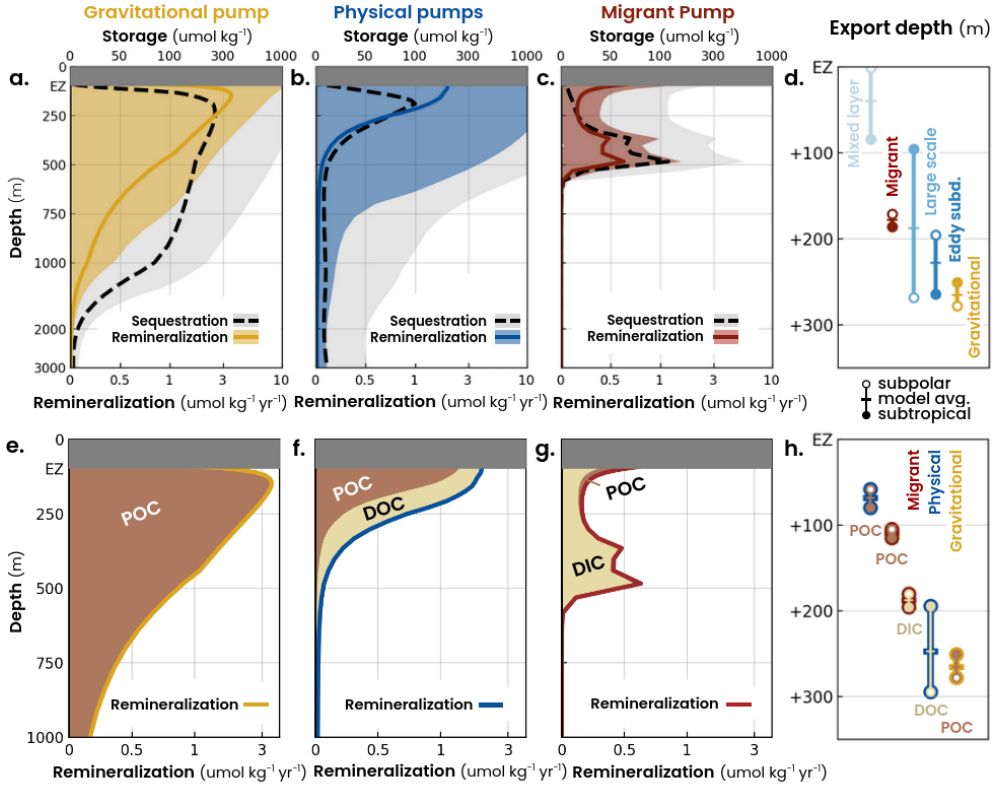


Fig. 4 (a–c) Annual-mean vertical profiles of carbon remineralization rates (solid yellow, blue and red lines) and storage (black dashed lines) associated with the (a) gravitational, (b) physical and (c) migrant pumps. Shading indicates ± 1 standard deviation of the annual spatial variability. The annual-mean euphotic zone (EZ, defined as the depth of 0.1% of surface irradiance) is shown in gray. (d) Export depth of carbon below the euphotic zone for the migrant pump (red), mixed-layer pump (light blue), large-scale pump (blue), eddy-subduction pump (dark blue) and gravitational pump (yellow). Horizontal lines show the model domain average (excluding convective region; see Methods); empty circles indicate the subpolar average and filled circles the subtropical average. (e–g) Annual-mean vertical profiles of carbon remineralization partitioned into particulate organic carbon (POC, brown) and dissolved carbon (pale yellow). (e) The gravitational pump (yellow line) transports only POC. (f) Physical pumps (blue line) transport both particulate and dissolved organic carbon. (g) The migrant pump (red line) injects dissolved inorganic carbon (DIC) through zooplankton respiration and particulate organic carbon (POC) through egestion and mortality; DOC excretion also occurs but is too small to be visible. (h) Export depth of particulate (brown) and dissolved (pale yellow) carbon below the EZ for the migrant (red), physical (blue) and gravitational (yellow) pumps.

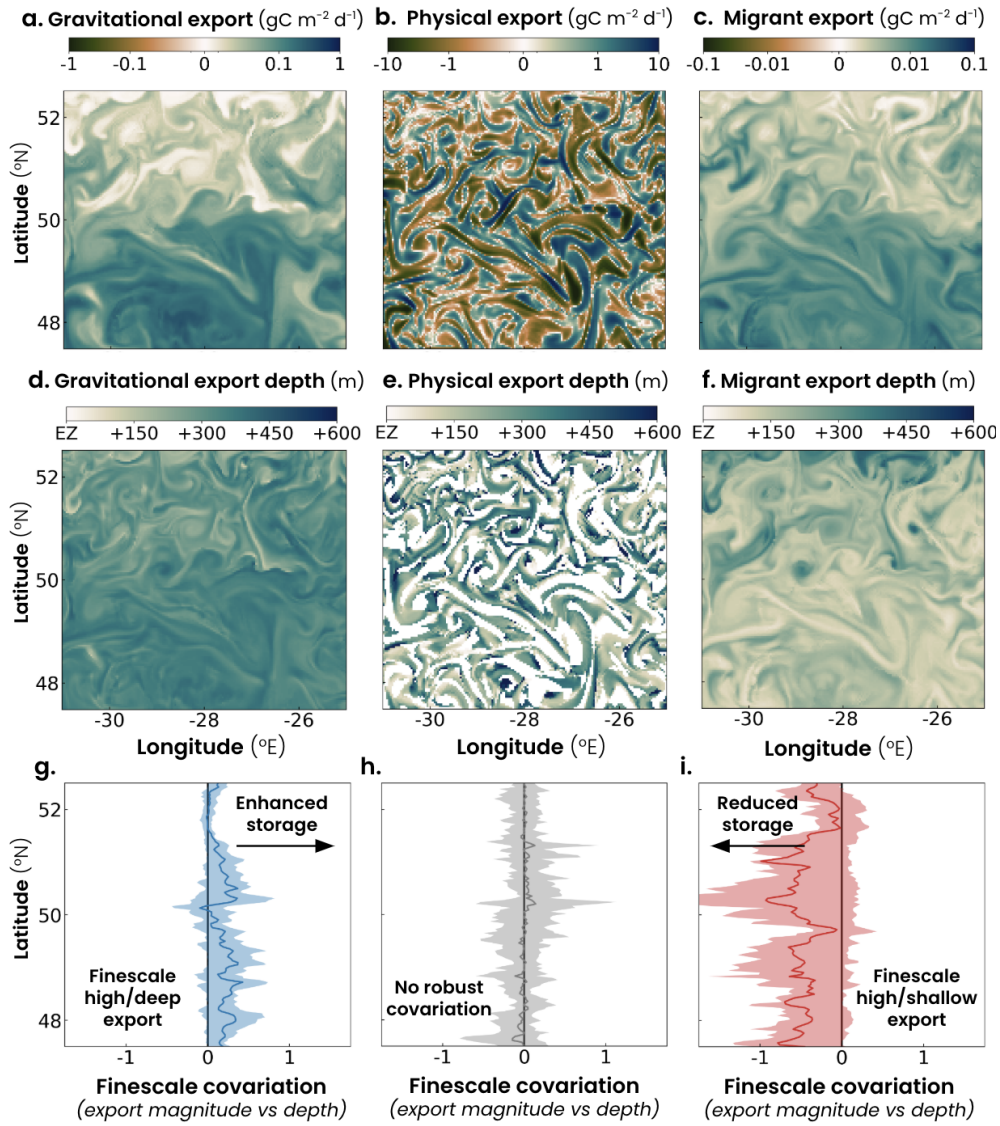


Fig. 5 Snapshots of carbon export by the (a) gravitational, (b) physical, and (c) migrant pumps on 10 March in the subpolar biome (31°W – 25°W , 48.5°N – 52.5°N ; same region as Fig. 2a–b). Positive values indicate export of carbon from the euphotic to the mesopelagic zone, whereas negative values indicate a supply of carbon from the mesopelagic into the euphotic zone. (d–f) Snapshots of the corresponding carbon export depth for the (d) gravitational, (e) physical, and (f) migrant pumps, respectively, with larger values indicating deeper export relative to the base of the euphotic zone (EZ). (g–i) Meridional profiles of finescale covariation between carbon export and export depth (see Methods), where negative values correspond to finescale structures that jointly increase export magnitude and decrease export depth (reducing carbon storage), and positive values indicate finescale patterns in which high export is associated with deep export depths (enhancing storage).

303 **7 Methods**

304 **Model description**

305

306 The study uses an idealized double gyre model reproducing the North Atlantic dynam-
307 ics, described in Poupon et al. (2025)[39]. This model couples an ocean physical model
308 (Modular Ocean Model version 6)[63], developed by the Geophysical Fluid Dynamics
309 Laboratory, with a biogeochemical module detailed below. The model domain is a box
310 3570 km side length and 4 km deep, centred around 40°N. To better represent fine-
311 scale dynamics, we increased the horizontal resolution from 9 km to 3 km compared to
312 Poupon et al. (2025)[39], with updated model parameters available in supplementary
313 (Table A1). This 3 km model is initialized from outputs of the 9 km model run for
314 100 years. The 3 km model is then spun-up for 25 years. The surface of the model is
315 continuously forced by an idealized seasonal cycle, including a sinusoidal zonal wind
316 profile inducing a double gyre circulation.

317

318 The physical model is coupled to the COBALTv2-DVM (Carbon, Ocean Bioge-
319 ochemistry and Lower Trophics version 2 with Diel Vertical Migration) biogeochemical
320 module [39, 64]. This module features 45 biogeochemical tracers, including the main
321 nutrients (i.e. nitrogen, phosphorus, silica, and iron) and a planktonic ecosystem com-
322 posed of 3 phytoplankton and 5 zooplankton, 3 non-migrating and 2 migrating. This
323 module represents the dynamics of suspended particulate organic carbon, in the form
324 of a planktonic ecosystem, sinking organic carbon in the form of detritus produced by
325 phytoplankton aggregation or zooplankton egestion and mortality. The sinking speed
326 of particles is 100 m d⁻¹[65] and their remineralization rate ranges between 0.02-0.5
327 d⁻¹ depending on temperature and oxygen concentration[66]. The amount of calcium
328 and silica composing the particles also modulates the remineralization rate, function-
329 ally reproducing a ballast/shielding effect that allows particles to sink deeper before
330 being remineralized[64]. The module also represents dissolved inorganic carbon and
331 four pools of dissolved organic carbon (labile, semi-labile, refractory, and background
332 ultrarefractory). Labile dissolved organic carbon is remineralized over a few days,
333 semi-labile over 90 days, and refractory over 10 years. The background DOC pool,
334 with a prescribed concentration of 46 μmol kg⁻¹, represents the refractory to ultra-
335 refractory fraction of Atlantic DOC, non-reactive over the timescales considered in our
336 experiment, as its degradation times exceed those of the overturning circulation. The
337 COBALTv2-DVM module also explicitly represents the diel vertical migration of zoo-
338 plankton as well as their compartmentalized physiology that temporally and spatially
339 decouples ingestion, digestion, respiration, and growth.

340 **Model biomes**

341

342 The model replicates the dynamics of a low-productivity, low-seasonality subtropical
343 biome and a high-productivity, high-seasonality subpolar biome typical of the North

344 Atlantic Ocean. The subtropical biome is defined by an annual mean surface chloro-
345 phyll concentration below 0.15 mg m^{-3} . The subpolar biome is defined by a mean
346 chlorophyll concentration above 0.35 mg m^{-3} and a mean mixed layer depth below
347 200 meters, to exclude model regions where deep convection is too strong and repre-
348 sentative of dynamics occurring in the Norwegian and Greenland seas (see Poupon et
349 al. 2025[39]).

350 Observations and validation

351

352 To evaluate the spatial and temporal variability of the biogeochemical dynamics sim-
353 ulated by the double-gyre model, we use satellite, ship-based, and float observations.
354 The mixed layer depth is calculated from hydrographic profiles collected between 1941
355 and 2022 [67], migrating zooplankton biomass from LIDAR measurements between
356 2007 and 2019 [68], and nets collected at the Bermuda Atlantic Time Series (BATS)
357 station between 1994 and 2010 [69]. Net primary productivity estimates are produced
358 by three algorithms (Eppley, CbPM, and CAFE) applied to Moderate-Resolution
359 Imaging Spectroradiometer measurements between 2002 and 2023 [70–72], and vali-
360 dated against in-situ measurements by the original authors. POC profiles come from
361 optical backscatter measurements collected by Biogeochemical-Argo floats between
362 2010 and 2021[73], DIC profiles from the GLODAPv2.2023 database [74], and DOC
363 profiles from a GEOTRACES compilation of ship measurements ranging from 1994
364 to 2021 [75].

365 Framework description

366 Carbon remineralization and storage

367

368 In our model, the total organic carbon remineralization ($\text{gC m}^{-3} \text{ yr}^{-1}$) which produces
369 dissolved inorganic carbon is the sum of the remineralization of particulate and organic
370 carbon by bacteria, and the respiration of migrating and non-migrating plankton:

$$\begin{aligned} \text{Remineralization}(z) = & \text{POC remineralization}(z) + \text{DOC remineralization}(z) \\ & + \text{Biological respiration}(z) \end{aligned} \quad (1)$$

371 We derive carbon storage (gC m^{-3}) as the product of this remineralization rate
372 and carbon storage time (yr) in subtropical and subpolar biomes from the Ocean
373 Circulation Inverse Model (OCIM) [6]):

$$\text{Storage}(z) = \text{Remineralization}(z) \times \text{Storage time}(z) \quad (2)$$

374 The amount of carbon stored in the water column corresponds to the vertical inte-
375 gral of this storage profile. Because the idealized geometry of our model does not
376 allow a one-to-one spatial mapping to OCIM, we approximate biome-scale storage by

multiplying the biome-mean storage time profile from OCIM with the biome-mean remineralization profile from our model. Evaluating the difference between the mean of the product ($\int \text{Remineralization}(z) \times \text{Storage time}(z) dz$) and the product of the means ($\overline{\int \text{Remineralization}(z) dz} \times \overline{\text{Storage time}(z) dz}$) using OCIM output indicates that this approximation leads to a modest underestimation of vertically integrated storage on the order of 3–5%.

We define the carbon export as the amount of carbon remineralized below the euphotic zone depth, defined as 0.1% of the photosynthetically active radiation at the surface [76]:

$$\text{Export} = \int_{\text{Euphotic Depth}}^{\text{Bottom}} \text{Remineralization}(z) dz \quad (3)$$

We further define the mean export depth (m) as the remineralization-weighted depth of exported carbon:

$$z_{\text{export}} = \frac{1}{\text{Export}} \int_{\text{Euphotic Depth}}^{\text{Bottom}} z \times \text{Remineralization}(z) dz \quad (4)$$

The mean remineralization depth associated with each export pathway (see following sections) is computed using the same expression, applied to the remineralization profile sustained by that pathway.

Carbon export pathways

The contribution of export pathways (gravitational, physical, migrant) to carbon remineralization is calculated considering that their organic carbon supply balances the remineralization flux:

$$\text{Biological respiration} = \text{Migrant respiration} + \text{Non-Migrant respiration} \quad (5)$$

$$\begin{aligned} \text{POC remineralization} = & -w_g \frac{\partial \text{POC}}{\partial z} - \vec{v} \cdot \vec{\nabla} \text{POC} + K_H \nabla_H^2 \text{POC} \\ & + \frac{\partial}{\partial z} \left(K_z \frac{\partial \text{POC}}{\partial z} \right) + \text{POC production} - \frac{\partial \text{POC}}{\partial t} \end{aligned} \quad (6)$$

$$\begin{aligned} \text{DOC remineralization} = & -\vec{v} \cdot \vec{\nabla} \text{DOC} + K_H \nabla_H^2 \text{DOC} \\ & + \frac{\partial}{\partial z} \left(K_z \frac{\partial \text{DOC}}{\partial z} \right) + \text{DOC production} - \frac{\partial \text{POC}}{\partial t} \end{aligned} \quad (7)$$

396 DOC and POC are the concentrations of dissolved and particulate organic carbon,
 397 $v = (u, v, w)$ is the fluid velocity, w_g is the gravitational sink velocity relative to
 398 the fluid, K_H and K_z are the horizontal and vertical diffusion coefficients. POC and
 399 DOC are produced by both migrating and non-migrating animals (egestion, excretion,
 400 mortality). Below the euphotic zone, production by non-migrant animals is marginal
 401 and can be neglected. On an annual average, the gyre is close to equilibrium. As a
 402 result, $d\text{DOC}/dt$ and $d\text{POC}/dt$ are also marginal and can be neglected. Thus, the
 403 carbon remineralization equation (1) can be written:

$$\begin{aligned} \text{Remineralization}(z) = & \text{ Gravitational pathway}(z) + \text{Physical pathway}(z) \\ & + \text{Migrant pathway}(z) \end{aligned} \quad (8)$$

404 With:

$$\text{Gravitational pathway} = -w_g \frac{\partial \text{POC}}{\partial z} \quad (9)$$

$$\begin{aligned} \text{Physical pathway} = & -\vec{v} \cdot \vec{\nabla} \text{POC} + K_H \nabla_H^2 \text{POC} + \frac{\partial}{\partial z} \left(K_z \frac{\partial \text{POC}}{\partial z} \right) \\ & - \vec{v} \cdot \vec{\nabla} \text{DOC} + K_H \nabla_H^2 \text{DOC} + \frac{\partial}{\partial z} \left(K_z \frac{\partial \text{DOC}}{\partial z} \right) \end{aligned} \quad (10)$$

$$\text{Migrant pathway} = \text{Migrant respiration} + \text{Migrant POC and DOC production} \quad (11)$$

405 Physical pathway decomposition

406
 407 The physical export pathway encompasses transport by large-scale circulation such as
 408 Ekman transport or overturning circulation (large-scale pathway), subduction induced
 409 by finescale structures such as sub-mesoscale fronts and mesoscale eddies (eddy sub-
 410 duction pathway), and transport induced by mixed layer deepening and restratification
 411 (mixed layer pathway).

$$\begin{aligned} \text{Physical pathway} = & \text{ Large scale pathway} + \text{Eddy-subduction pathway} \\ & + \text{Mixed layer pathway} \end{aligned} \quad (12)$$

412 We isolate the small and large advective components using a Reynold's
 413 decomposition[77]:

$$\overline{C\vec{v}} = \overline{C} \vec{v} + \overline{C'\vec{v}'} \quad (13)$$

414 Where $(\overline{\cdot})$ is a gaussian spatial mean operator with a radius of 100 km and $(')$ the
 415 small scale residual. We isolate the vertical mixing in the mixing layer from the mixing
 416 in the interior ocean using an indicator function ($Ind_{z < MLD}$), which takes the value
 417 1 for depths within the mixed layer and 0 otherwise, and vice versa for ($Ind_{z > MLD}$).
 418 This way, the three pathways of the physical pump are:

$$\begin{aligned}
 \text{Large scale pathway} = & -\vec{\nabla} \cdot (\bar{\vec{v}} \overline{POC} + \bar{\vec{v}} \overline{DOC}) + K_H \nabla_H^2 (POC + DOC) \\
 & + \frac{\partial}{\partial z} \left(K_z \left(\frac{\partial POC}{\partial z} + \frac{\partial DOC}{\partial z} \right) \right) \times Ind_{z > MLD}
 \end{aligned} \quad (14)$$

$$\text{Eddy subduction pathway} = -\vec{\nabla} \cdot (\bar{\vec{v}'} \overline{POC'} + \bar{\vec{v}'} \overline{DOC'}) \quad (15)$$

$$\text{Mixed layer pathway} = \frac{\partial}{\partial z} \left(K_z \left(\frac{\partial POC}{\partial z} + \frac{\partial DOC}{\partial z} \right) \right) \times Ind_{z < MLD} \quad (16)$$

419 This framework makes it possible to quantify not only the various components of
 420 the biological carbon pump, but also their respective spatial and temporal variability
 421 across all space and time scales.

422 Finescale covariation factor

423 To highlight how finescale dynamics jointly modulate carbon export magnitude and
 424 export depth, we decomposed each variable into a large-scale background field and
 425 a finescale anomaly, using the same gaussian spatial mean operator described above
 426 $(\overline{\cdot})$. For each export pathway, the export flux e and export depth d were written
 427 as $e = \bar{e} + e'$ and $d = \bar{d} + d'$, where \bar{e} and \bar{d} denote the large-scale components
 428 obtained via Reynold's decomposition, and e' and d' represent the finescale residuals.
 429 We then defined a finescale covariation factor that measures the local co-fluctuation
 430 of anomalies in export magnitude and export depth. This factor is computed as

$$C = \frac{e'}{\sigma_e} \times \frac{d'}{\sigma_d} \quad (17)$$

432 where σ_e and σ_d are the standard deviations of the finescale export and depth
 433 anomalies over the gaussian filter domain. Positive values of C indicate that finescale
 434 structures simultaneously enhance export magnitude and deepen export (or reduce
 435 export magnitude and shoal export), whereas negative values indicate opposite-signed
 436 anomalies.

437 **Acknowledgements.** We thank Gaby Negrete-Garcia for conducting the Geophysical
 438 Fluid Dynamics Laboratory internal review.

439 **Declarations**

440 **Funding.** The study has been supported by the National Science Foundation (Eddy
441 effects on Biological Pump award number 2023108).

442 **Competing interest.** The authors declare no competing interests.

443 **Data and Code availability.** The COBALTv2-DVM model and idealized
444 double gyre configuration presented in this paper are available on github at
445 https://github.com/mpoupon/MOM6_Double_Gyre.

446 **Author contribution.** Conceptualization: MP, LR, JL. Data curation: MP. For-
447 mal analysis: MP. Funding acquisition: LR, JL. Investigation: MP. Methodology: MP.
448 Software: MP. Supervision: LR, JL. Visualization: MP. Writing – original draft: MP.
449 Writing – review and editing: MP, LR, JL.

450 Appendix A

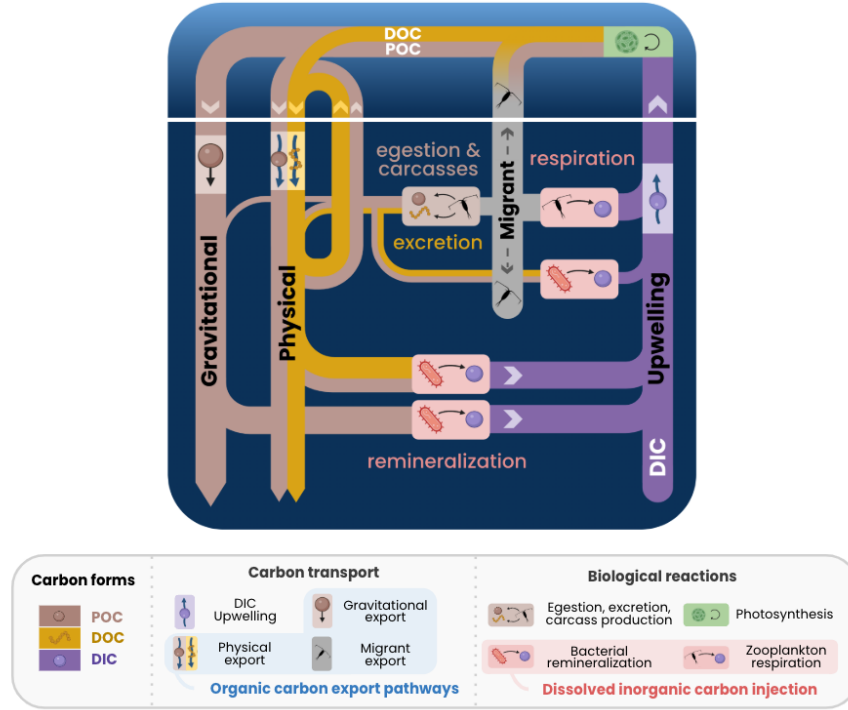


Fig. A1 Interconnection of the biological carbon pumps. Dissolved and particulate organic carbon is produced in the euphotic zone after photosynthesis (green block). The gravitational pump exports carbon out of the euphotic zone (white line) via gravitational settling. The physical pumps export the particles and the dissolved carbon via oceanic transport. The migrant pump exports carbon via respiration, the production of particles by egestion (fecal pellets) or mortality (carcasses), and the production of dissolved organic carbon (excretion) by the zooplankton migrating below the euphotic zone. The particles produced can then be exported deeper by the gravitational and physical pumps, while the dissolved organic carbon can be transported deeper by the physical pump. This export sustains remineralization and injects DIC into the mesopelagic zone. The DIC from remineralization is stored in the interior ocean before being brought back to the surface by oceanic transport.

Eddy kinetic energy ($\text{cm}^2 \text{ s}^{-2}$)

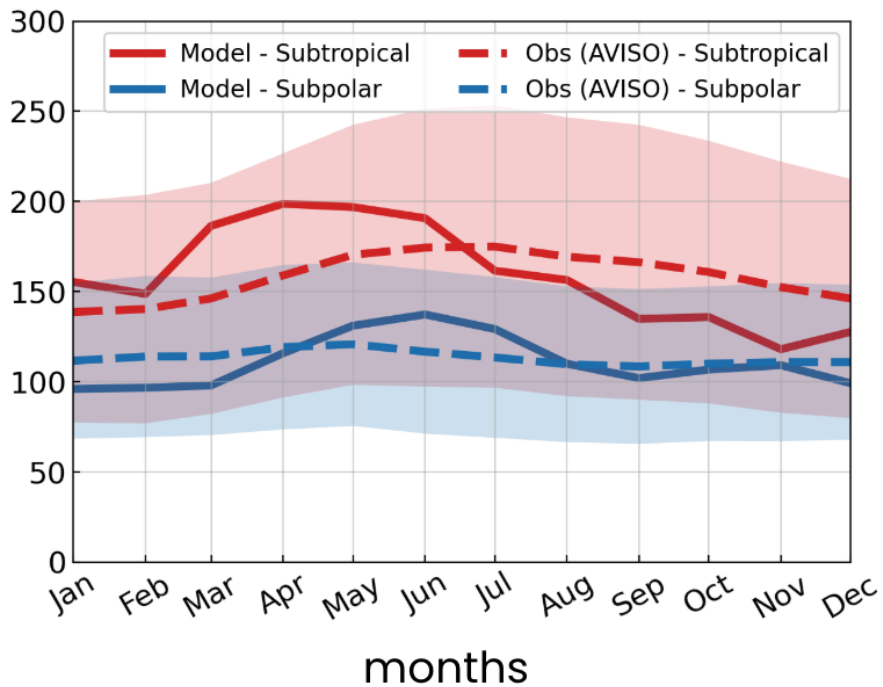


Fig. A2 Seasonal cycle of observed (dashed lines AVISO product) and modeled (solid lines) eddy kinetic energy in the subtropical (red) and subpolar (blue) biome. Shading represents the spatial variability of monthly values within the biomes (one standard deviation).

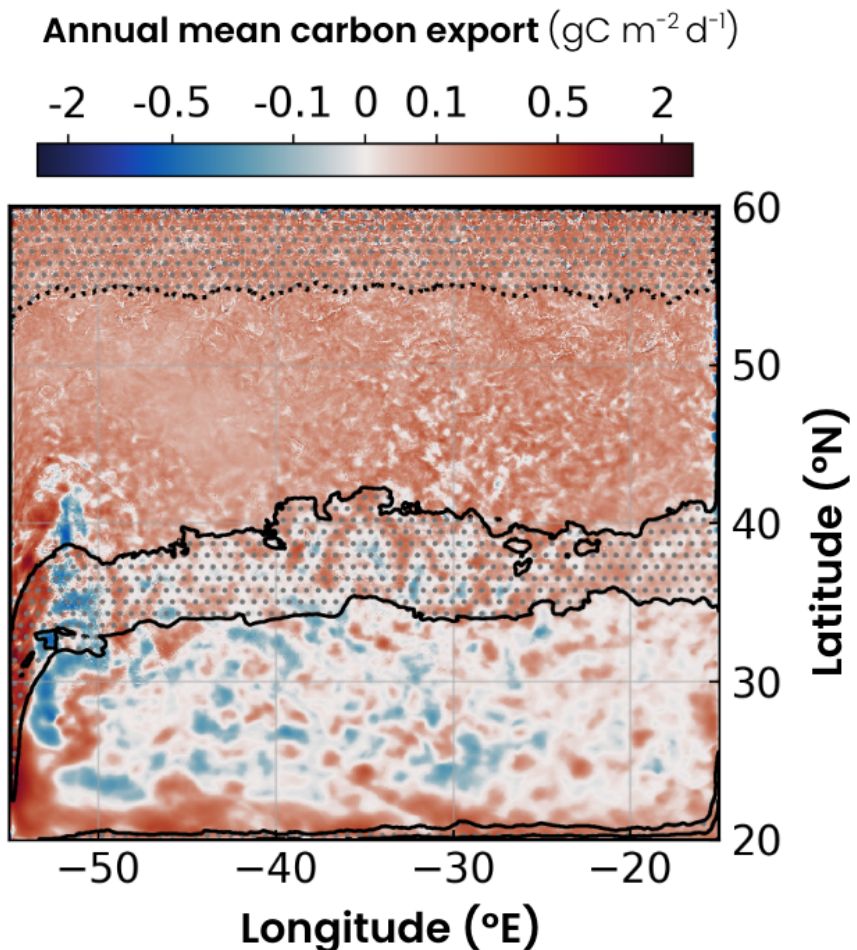


Fig. A3 Biological carbon export annual average in the double gyre model. Subtropical and subpolar biomes are defined by annual chlorophyll concentrations lower than 0.15 mg m^{-3} and higher than 0.35 mg m^{-3} respectively (black lines). Deep convection ($\sim 55\text{--}60^{\circ}\text{N}$) region defined by an annual mixed layer depth $> 150 \text{ m}$, and the jet region ($\sim 35\text{--}40^{\circ}\text{N}$) defined by chlorophyll concentrations between $0.15\text{--}0.35 \text{ mg m}^{-3}$, are excluded from the biome analysis (dotted areas).

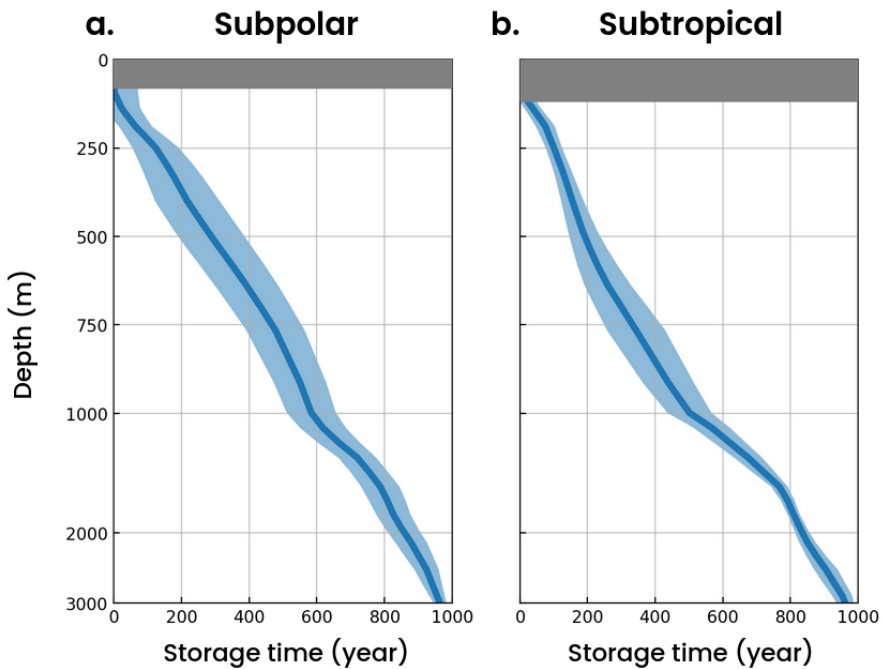


Fig. A4 Vertical profile of remineralized carbon storage time in the interior ocean in (a) the subpolar biome and (b) the subtropical biome from the OCIM model [6]. The fillings show the annual spatial variability of each pump within the biomes (two standard deviations). Grey boxes are the mean euphotic zone (EZ) extending down to the depth where irradiance is 0.1% of surface irradiance: 85m in the subpolar biome and 115 m in the subtropical biome.

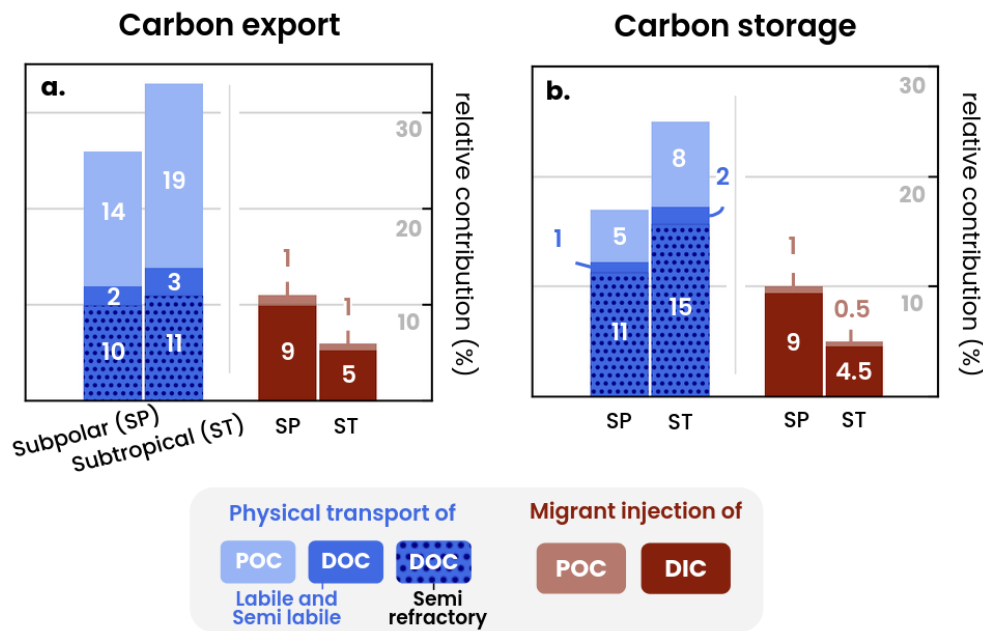


Fig. A5 Relative contribution of dissolved and particulate fluxes to (a) carbon export and (b) carbon storage by physical (blue) and migrant (red) pumps. Physical pumps export and store particulate carbon (light blue), labile and semi-labile dissolved carbon (dark blue) and semi-recalcitrant carbon (dark blue to point). The migrating pump exports and stores particulate carbon produced by the egestion or death of zooplankton (light red) as well as the respiration of zooplankton migrating along its migration trajectory (dark red).

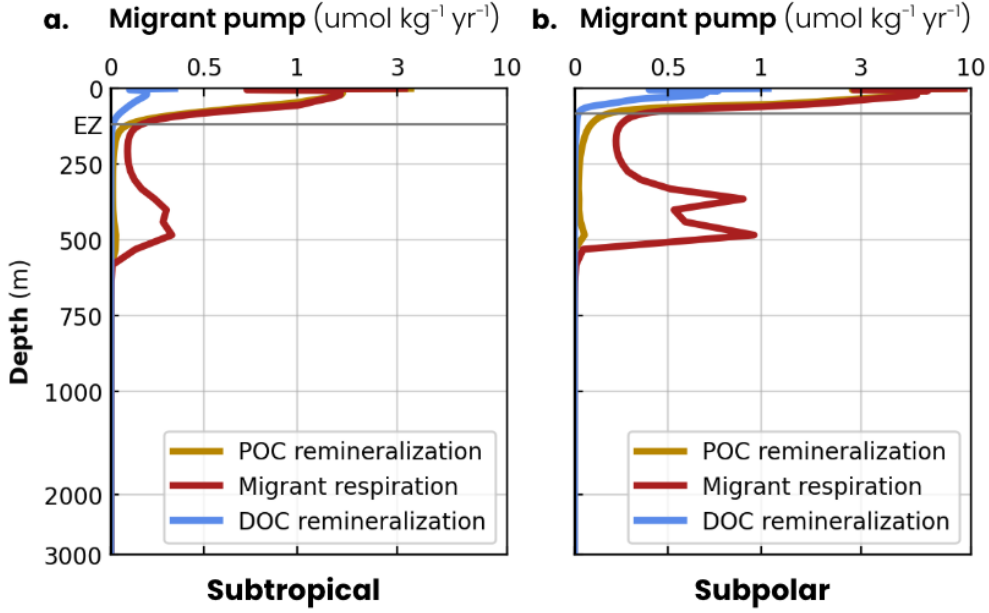


Fig. A6 Average annual vertical profile of remineralized carbon by the migrant pump in (a) subtropical and (b) subpolar biomes. Remineralization is supported by the production of organic particles (e.g., particle or carcass management, brown line), DOC production (excretion, blue line), and respiration by migrant zooplankton (red line). The euphotic zone (EZ) boundary in both biomes is represented by a horizontal gray line.

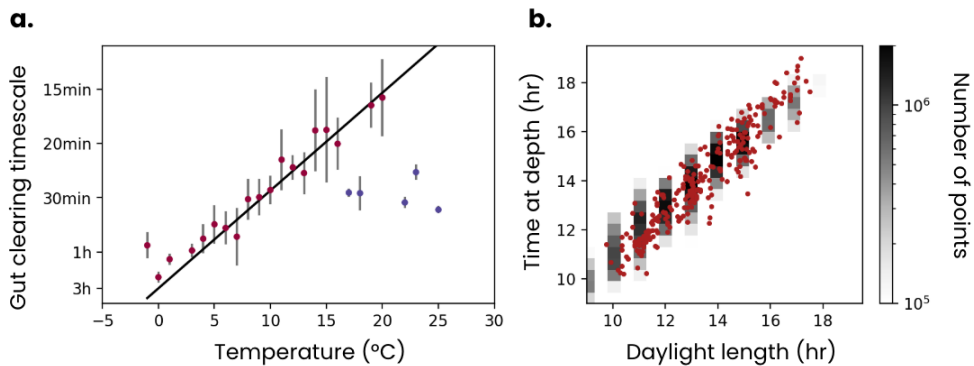


Fig. A7 (a) Time scale of gut clearance observed by Irigoien ([43], dots) and modeled in the COBALTv2-DVM model (black line) as a function of temperature. Observations are binned by degree of temperature and the gray lines represent a standard deviation. (b) Time spent at depth by migrating zooplankton as a function of the duration of daylight in the model (black shading) and the observation-based data product compiled by Bianchi et al. (2016[78], red dots).

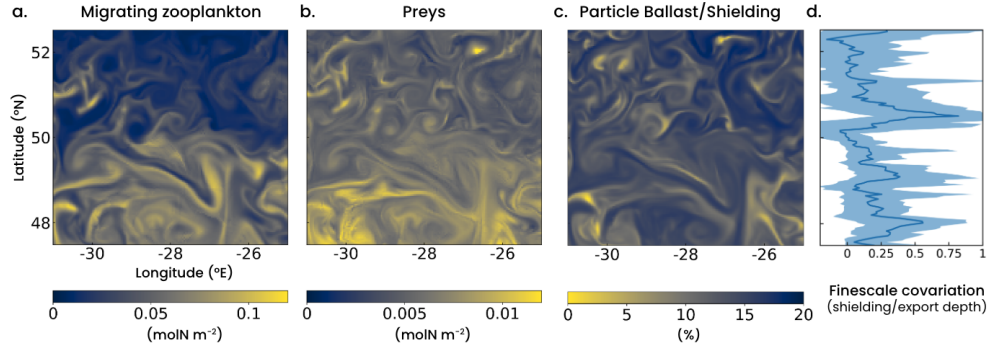


Fig. A8 (a–c) Snapshots on 10 March of the subpolar biome (31°W – 25°W , 48.5°N – 52.5°N ; same region as Fig. A8a–b) showing the nitrogen content of (a) migrating zooplankton and (b) their prey, together with (c) the local particle ballast/shielding factor expressed as the relative contribution of calcifying and silicifying plankton to total particulate nitrogen. Fine-scale eddies and fronts generate strong spatial heterogeneity in all three fields. (d) Meridional section of the finescale covariation between particle shielding and gravitational export depth, computed as the normalized product of their small-scale anomalies. Positive values indicate locations where enhanced particle shielding is associated with deeper export, jointly amplifying carbon storage.

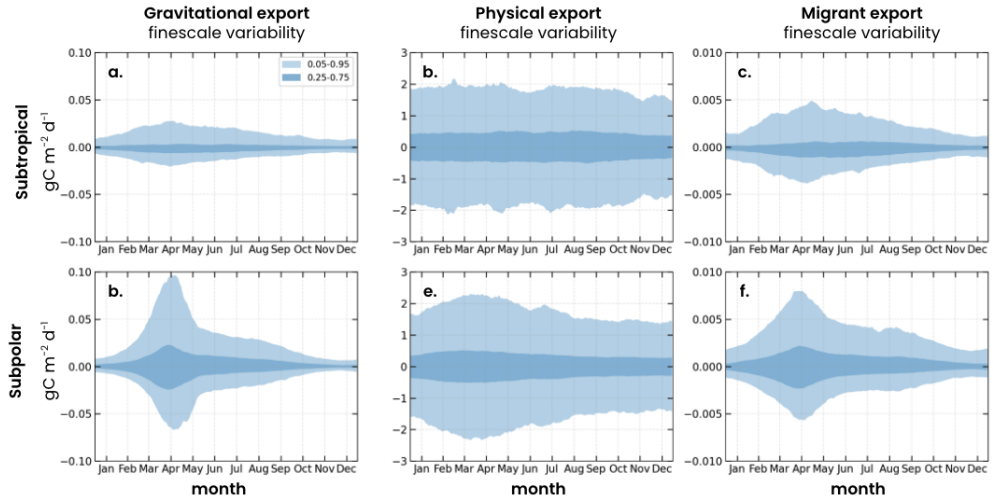


Fig. A9 Seasonal evolution of the finescale component of gravitational, physical, and migrant carbon export in the subtropical (top row) and subpolar (bottom row) biomes. For each pump, the shaded envelopes show the distribution of finescale anomalies across the domain: the light shading denotes the 0.05–0.95 quantile range and the darker shading the 0.25–0.75 quantile range.

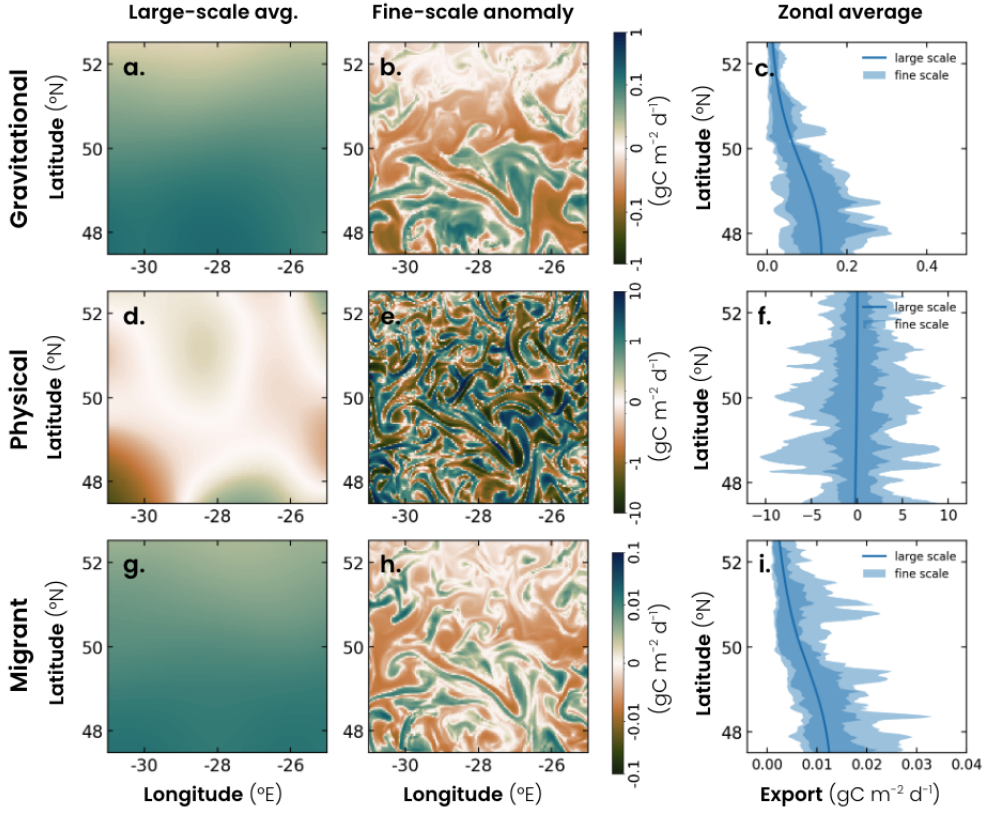


Fig. A10 Snapshots on 10 March in the subpolar biome (31° W– 25° W, 48.5° N– 52.5° N; same region as Fig. 2a–b) illustrating the decomposition of gravitational, physical, and migrant export into large-scale and finescale components. (a,d,g) Large-scale fields obtained by spatial filtering, capturing the smooth background structure of each export pathway. (b,e,h) Corresponding finescale anomalies, defined as the deviation from the large-scale field and highlighting the filamentary eddy- and front-driven variability. (c,f,i) Zonal averages showing the meridional structure of both components: the solid line is the large-scale mean, while the shaded envelopes show the finescale distribution across longitudes (light shading = 0.05–0.95 quantiles; dark shading = 0.25–0.75 quantiles).

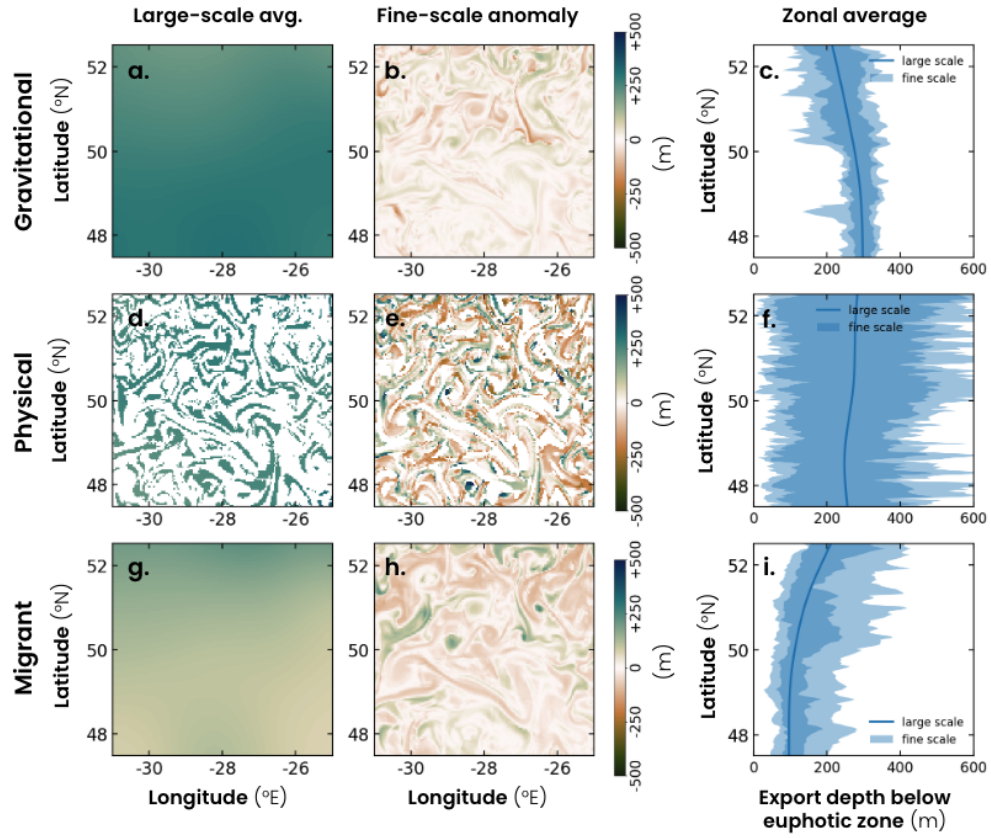


Fig. A11 Snapshots on 10 March in the subpolar biome (31°W – 25°W , 48.5°N – 52.5°N ; same region as Fig. 2a–b) showing the decomposition of gravitational, physical, and migrant export depth into their large-scale and finescale components. (a,d,g) Large-scale export depth, obtained by spatial filtering and representing the smooth background pattern of how deep carbon is exported below the base of the euphotic zone. (b,e,h) Corresponding finescale anomalies, defined as deviations from the large-scale field, highlighting eddy- and front-driven modulation of export depth. Positive anomalies indicate locally deeper export pathways, negative anomalies shallower export. (c,f,i) Zonal averages summarizing the meridional structure of export depth: the solid line shows the large-scale mean, while the shaded envelopes represent the distribution of finescale variability across longitudes (light shading = 0.05–0.95 quantiles; dark shading = 0.25–0.75 quantiles).

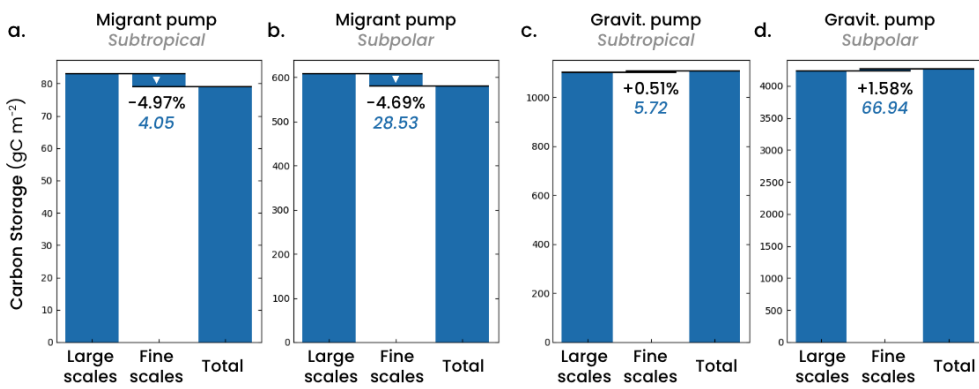


Fig. A12 Large-scale, finescale, and total carbon storage associated with the migrant pump (a–b) and gravitational pump (c–d) in the subtropical and subpolar biomes. For each pump and biome, the left bar shows the storage obtained from the large-scale component, the middle bar the contribution of finescale dynamics, and the right bar the total storage. Percent values above the middle bars indicate the relative finescale contribution, expressed as a percentage of the total, and the numbers in blue show its absolute magnitude (gC m^{-2}). Finescale processes slightly reduce the migrant pump storage (a–b) but enhance the gravitational pump storage (c–d), with larger finescale impacts in the subpolar biome.

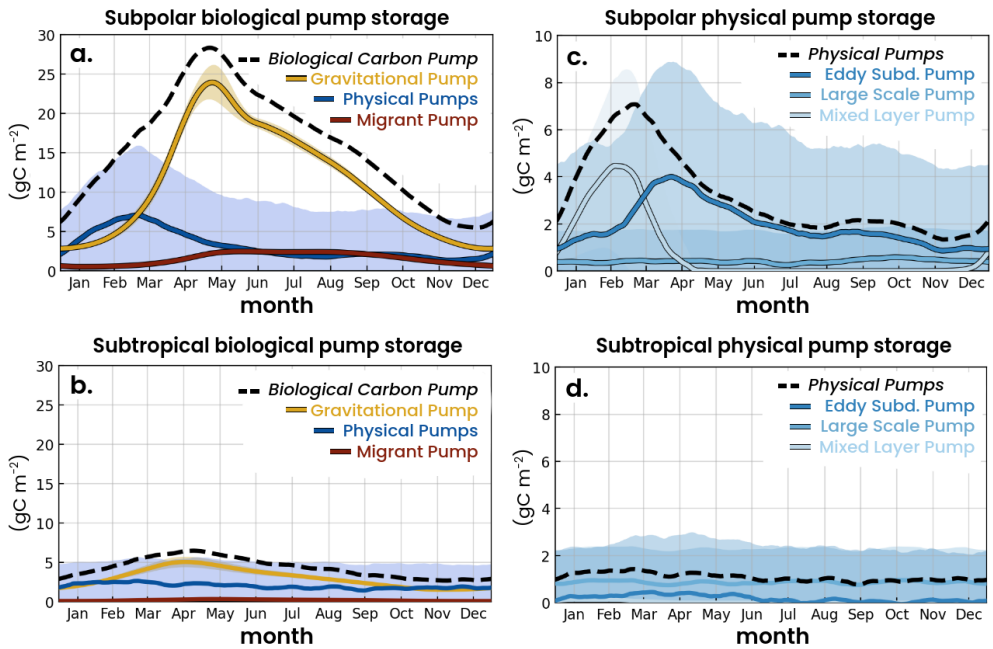


Fig. A13 (a-b) Seasonal cycle of carbon storage by the biological carbon pump (black dashed line) in (a) the subpolar and (b) the subtropical biomes, defined as the sum of the gravitational (yellow), physical (blue) and migrant (red) pumps. (c-d) Seasonal cycle carbon storage by the physical pumps (black dashed line) in the (c) subpolar and (d) subtropical biomes, decomposed into the eddy-subduction (dark blue), large-scale (blue) and mixed-layer (light blue) components. Shading denotes the intra-biome spatial variability at daily resolution (± 2 standard deviations).

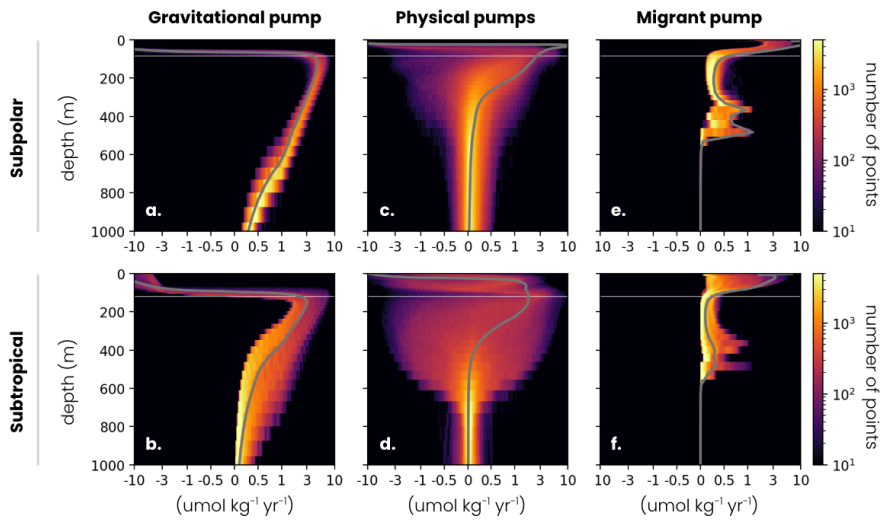


Fig. A14 Annual carbon remineralization vertical distribution in (top row) the subpolar biome and (bottom row) the subtropical biome by (a,b) the gravitational pump, (c,d) the physical pumps and (e,f) the migrant pump. The gray lines is the annual average value.

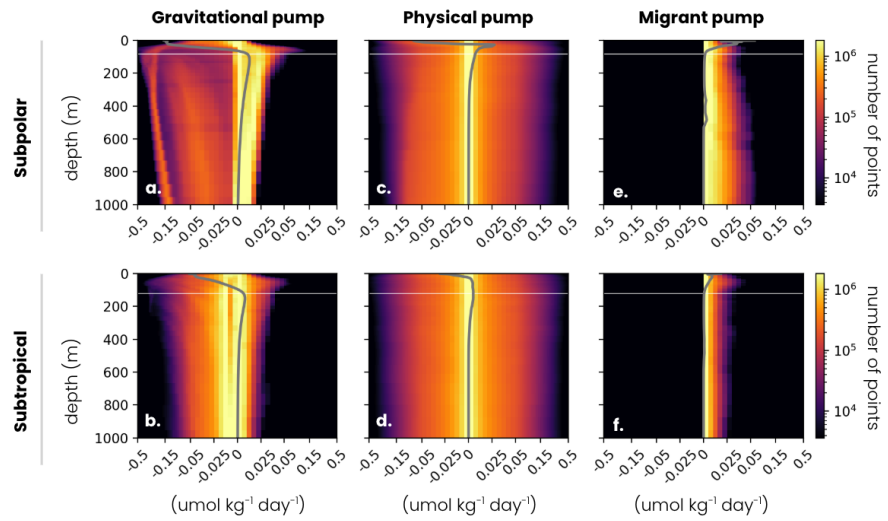


Fig. A15 Daily carbon remineralization vertical distribution in (top row) the subpolar biome and (bottom row) the subtropical biome by (a,b) the gravitational pump, (c,d) the physical pumps and (e,f) the migrant pump. The gray lines is the annual average value.

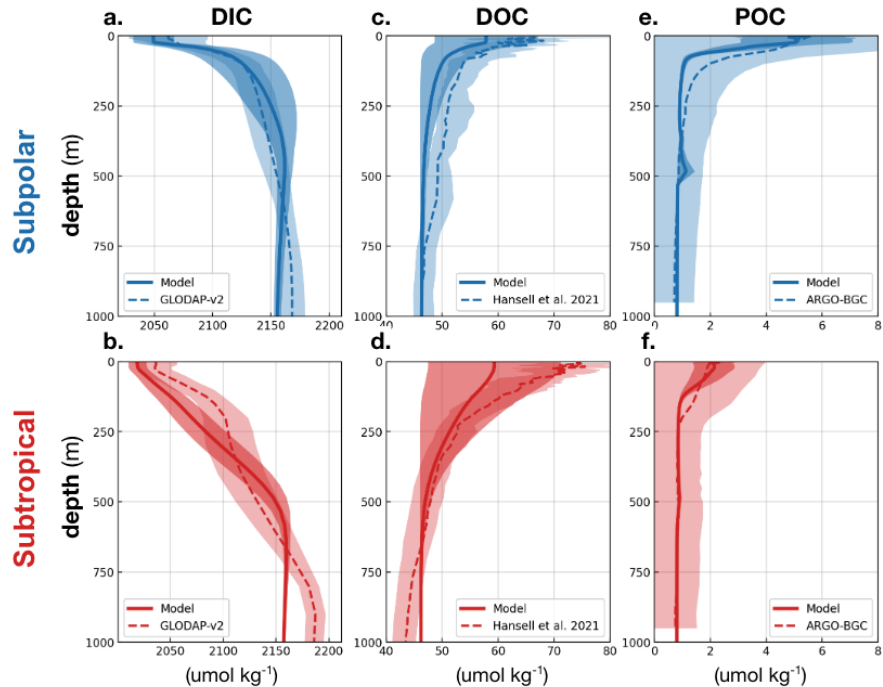


Fig. A16 Vertical profiles of annual (a,b) dissolved inorganic carbon, (c,d) dissolved organic carbon and (e,f) particulate organic carbon concentrations (dotted line) observed and (solid line) modeled in (a,c,e) the subpolar biome and (b,d,f) the subtropical biome. Shading is the spatial variability of this annual average within the biome (one standard deviation).

Table A1 Major parameters and associated values used in the physical ocean component of the model

Parameter	Values	References
Horizontal grid and resolution	1082 x 1082, 3.1 km	
Vertical coordinate	75 layer hybrid z*-isopycnal	(Adcroft et al. 2019)
Number of CPUs	1024	
Baroclinic and Biogeochemical time steps	100 s, 300 s	
Planetary boundary layer parameterization	ePBL	(Reichl and Hallberg. 2018)
Subgrid Mesoscale EKE parameterization	No	(Hallberg et al. 2013)
Submesoscale restratification parameterization	Frontal length = 1500 m	(Fox-Kemper et al. 2008)
Background kinematic viscosity	$K_V=10^{-6} \text{ m}^2.\text{s}^{-1}$	
Background diapycnal diffusivity	$K_D=10^{-6} \text{ m}^2.\text{s}^{-1}$	
Horizontal viscosity	Smagorinsky biharmonic Smagorinsky coefficient = 0.015 Resolution-dependent = 0.01 $\Delta_x^3 \text{ m}^4\text{s}^{-1}$	(Griffies et al. 2000)
Opacity Scheme	3-band with chlorophyll	(Manizza et al. 2005)

451 **References**

- 452 [1] Volk, T., Hoffert, M.I.: Ocean Carbon Pumps: Analysis of Rela-
453 tive Strengths and Efficiencies in Ocean-Driven Atmospheric CO₂
454 Changes. In: The Carbon Cycle and Atmospheric CO₂: Natural
455 Variations Archean to Present, pp. 99–110. American Geophysical
456 Union (AGU), ??? (1985). <https://doi.org/10.1029/GM032p0099> .
457 _eprint: <https://onlinelibrary.wiley.com/doi/pdf/10.1029/GM032p0099> . Accessed
458 <https://onlinelibrary.wiley.com/doi/abs/10.1029/GM032p0099> . Accessed
459 2024-10-29
- 460 [2] Siegel, D.A., DeVries, T., Cetinić, I., Bisson, K.M.: Quantifying the
461 Ocean’s Biological Pump and Its Carbon Cycle Impacts on Global Scales.
462 Annual Review of Marine Science **15**(1), 329–356 (2023) <https://doi.org/10.1146/annurev-marine-040722-115226> . _eprint: <https://doi.org/10.1146/annurev-marine-040722-115226>. Accessed 2023-04-20
- 465 [3] Boyd, P.W., Claustre, H., Levy, M., Siegel, D.A., Weber, T.: Multi-faceted particle
466 pumps drive carbon sequestration in the ocean. Nature **568**(7752), 327–335 (2019)
467 <https://doi.org/10.1038/s41586-019-1098-2> . Number: 7752 Publisher: Nature
468 Publishing Group. Accessed 2022-01-30
- 469 [4] Henson, S.A., Sanders, R., Madsen, E.: Global patterns in efficiency of par-
470 ticulate organic carbon export and transfer to the deep ocean. Global Biogeoch-
471 emical Cycles **26**(1) (2012) <https://doi.org/10.1029/2011GB004099> . _eprint:
472 <https://onlinelibrary.wiley.com/doi/pdf/10.1029/2011GB004099>. Accessed 2023-
473 04-20
- 474 [5] Bopp, L., Resplandy, L., Orr, J.C., Doney, S.C., Dunne, J.P., Gehlen, M.,
475 Halloran, P., Heinze, C., Ilyina, T., Séférian, R., Tjiputra, J., Vichi, M.:
476 Multiple stressors of ocean ecosystems in the 21st century: projections with
477 CMIP5 models. Biogeosciences **10**(10), 6225–6245 (2013) <https://doi.org/10.5194/bg-10-6225-2013> . Publisher: Copernicus GmbH. Accessed 2022-10-16
- 479 [6] DeVries, T., Weber, T.: The export and fate of organic matter in
480 the ocean: New constraints from combining satellite and oceano-
481 graphic tracer observations. Global Biogeochemical Cycles **31**(3),
482 535–555 (2017) <https://doi.org/10.1002/2016GB005551> . _eprint:
483 <https://onlinelibrary.wiley.com/doi/pdf/10.1002/2016GB005551>. Accessed
484 2023-04-20
- 485 [7] Kwiatkowski, L., Torres, O., Bopp, L., Aumont, O., Chamberlain, M., Chris-
486 tian, J.R., Dunne, J.P., Gehlen, M., Ilyina, T., John, J.G., Lenton, A., Li, H.,
487 Lovenduski, N.S., Orr, J.C., Palmieri, J., Santana-Falcón, Y., Schwinger, J.,
488 Séférian, R., Stock, C.A., Tagliabue, A., Takano, Y., Tjiputra, J., Toyama, K.,
489 Tsujino, H., Watanabe, M., Yamamoto, A., Yool, A., Ziehn, T.: Twenty-first
490 century ocean warming, acidification, deoxygenation, and upper-ocean nutrient

- 491 and primary production decline from CMIP6 model projections. *Biogeosciences*
492 **17**(13), 3439–3470 (2020) <https://doi.org/10.5194/bg-17-3439-2020> . Publisher:
493 Copernicus GmbH. Accessed 2022-10-16
- 494 [8] Nowicki, M., DeVries, T., Siegel, D.A.: Quantifying the Car-
495 bon Export and Sequestration Pathways of the Ocean's Biological
496 Carbon Pump. *Global Biogeochemical Cycles* **36**(3), 2021–
497 007083 (2022) <https://doi.org/10.1029/2021GB007083> . eprint:
498 <https://onlinelibrary.wiley.com/doi/pdf/10.1029/2021GB007083>. Accessed
499 2023-04-20
- 500 [9] Carter, B.R., Feely, R.A., Lauvset, S.K., Olsen, A., DeVries, T., Son-
501 nerup, R.: Preformed Properties for Marine Organic Matter and Carbonate
502 Mineral Cycling Quantification. *Global Biogeochemical Cycles* **35**(1),
503 2020–006623 (2021) <https://doi.org/10.1029/2020GB006623> . eprint:
504 <https://onlinelibrary.wiley.com/doi/pdf/10.1029/2020GB006623>. Accessed
505 2024-11-25
- 506 [10] Henson, S.A., Laufkötter, C., Leung, S., Giering, S.L.C., Palevsky, H.I.,
507 Cavan, E.L.: Uncertain response of ocean biological carbon export in a chang-
508 ing world. *Nature Geoscience* **15**(4), 248–254 (2022) <https://doi.org/10.1038/s41561-022-00927-0> . Number: 4 Publisher: Nature Publishing Group. Accessed
509 2023-04-25
- 510 [11] Levy, M., Bopp, L., Karleskind, P., Resplandy, L., Ethe, C., Pin-
511 sard, F.: Physical pathways for carbon transfers between the surface
512 mixed layer and the ocean interior. *Global Biogeochemical Cycles*
513 **27**(4), 1001–1012 (2013) <https://doi.org/10.1002/gbc.20092> . eprint:
514 <https://onlinelibrary.wiley.com/doi/pdf/10.1002/gbc.20092>. Accessed
515 2022-08-22
- 516 [12] Gardner, W.D., Chung, S.P., Richardson, M.J., Walsh, I.D.: The oceanic mixed-
517 layer pump. *Deep Sea Research Part II: Topical Studies in Oceanography* **42**(2),
518 757–775 (1995) [https://doi.org/10.1016/0967-0645\(95\)00037-Q](https://doi.org/10.1016/0967-0645(95)00037-Q) . Accessed 2025-
519 04-11
- 520 [13] Dall'Olmo, G., Dingle, J., Polimene, L., Brewin, R.J.W., Claustre, H.: Substantial
521 energy input to the mesopelagic ecosystem from the seasonal mixed-layer pump.
522 *Nature Geoscience* **9**(11), 820–823 (2016) <https://doi.org/10.1038/ngeo2818> .
523 Number: 11 Publisher: Nature Publishing Group. Accessed 2023-04-21
- 524 [14] Omand, M.M., D'Asaro, E.A., Lee, C.M., Perry, M.J., Briggs, N., Cetinić,
525 I., Mahadevan, A.: Eddy-driven subduction exports particulate organic carbon
526 from the spring bloom. *Science* (2015) <https://doi.org/10.1126/science.1260062>
527 . Publisher: American Association for the Advancement of Science. Accessed
528 2022-01-30

- 530 [15] Resplandy, L., Lévy, M., McGillicuddy Jr., D.J.: Effects of Eddy-Driven Sub-
 531 duction on Ocean Biological Carbon Pump. *Global Biogeochemical Cycles*
 532 **33**(8), 1071–1084 (2019) <https://doi.org/10.1029/2018GB006125> . eprint:
 533 <https://onlinelibrary.wiley.com/doi/pdf/10.1029/2018GB006125>. Accessed 2023-
 534 04-20
- 535 [16] Mahadevan, A.: The Impact of Submesoscale Physics on Primary Pro-
 536 ductivity of Plankton. *Annual Review of Marine Science* **8**(1), 161–
 537 184 (2016) <https://doi.org/10.1146/annurev-marine-010814-015912> . eprint:
 538 <https://doi.org/10.1146/annurev-marine-010814-015912>. Accessed 2022-01-30
- 539 [17] Stukel, M.R., Aluwihare, L.I., Barbeau, K.A., Chekalyuk, A.M., Goericke, R.,
 540 Miller, A.J., Ohman, M.D., Ruacho, A., Song, H., Stephens, B.M., Landry, M.R.:
 541 Mesoscale ocean fronts enhance carbon export due to gravitational sinking and
 542 subduction. *Proceedings of the National Academy of Sciences* **114**(6), 1252–1257
 543 (2017) <https://doi.org/10.1073/pnas.1609435114> . Publisher: Proceedings of the
 544 National Academy of Sciences. Accessed 2023-04-20
- 545 [18] Stukel, M.R., Song, H., Goericke, R., Miller, A.J.: The role of subduction and
 546 gravitational sinking in particle export, carbon sequestration, and the remi-
 547 neralization length scale in the California Current Ecosystem. *Limnology and
 548 Oceanography* **63**(1), 363–383 (2018) <https://doi.org/10.1002/limo.10636> . eprint:
 549 <https://onlinelibrary.wiley.com/doi/pdf/10.1002/limo.10636>. Accessed 2023-04-21
- 550 [19] Steinberg, D.K., Carlson, C.A., Bates, N.R., Goldthwait, S.A., Madin, L.P.,
 551 Michaels, A.F.: Zooplankton vertical migration and the active transport of dis-
 552 solved organic and inorganic carbon in the Sargasso Sea. *Deep Sea Research
 553 Part I: Oceanographic Research Papers* **47**(1), 137–158 (2000) [https://doi.org/
 554 10.1016/S0967-0637\(99\)00052-7](https://doi.org/10.1016/S0967-0637(99)00052-7) . Accessed 2023-04-21
- 555 [20] Aumont, O., Maury, O., Lefort, S., Bopp, L.: Evaluating the Poten-
 556 tial Impacts of the Diurnal Vertical Migration by Marine Organisms
 557 on Marine Biogeochemistry. *Global Biogeochemical Cycles* **32**(11),
 558 1622–1643 (2018) <https://doi.org/10.1029/2018GB005886> . eprint:
 559 <https://onlinelibrary.wiley.com/doi/pdf/10.1029/2018GB005886>. Accessed
 560 2023-04-20
- 561 [21] Pinti, J., DeVries, T., Norin, T., Serra-Pompei, C., Proud, R., Siegel, D.A.,
 562 Kiørboe, T., Petrik, C.M., Andersen, K.H., Brierley, A.S., Visser, A.W.: Model
 563 estimates of metazoans' contributions to the biological carbon pump. *Bio-
 564 geosciences* **20**(5), 997–1009 (2023) <https://doi.org/10.5194/bg-20-997-2023> .
 565 Publisher: Copernicus GmbH. Accessed 2024-11-09
- 566 [22] Cuvier, G., Laurillard, C.L., Pierron, J.A., Louvet, G.P., Latreille,
 567 P.A.: *Le Règne Animal Distribué D'après Son Organisation : Pour
 568 Servir de Base a L'histoire Naturelle des Animaux et D'introduction a
 569 L'anatomie Comparée* vol. 1. Chez Déterville, A Paris (1817). Pages: 1-588.

- 570 <https://www.biodiversitylibrary.org/item/18030>
- 571 [23] Omand, M.M., Steinberg, D.K., Stamieszkin, K.: Cloud shadows drive vertical
572 migrations of deep-dwelling marine life. Proceedings of the National Academy of
573 Sciences **118**(32), 2022977118 (2021) <https://doi.org/10.1073/pnas.2022977118> .
574 Publisher: Proceedings of the National Academy of Sciences. Accessed 2023-04-24
- 575 [24] Wilson, J.D., Andrews, O., Katavouta, A., Melo Viríssimo, F., Death, R.M.,
576 Adloff, M., Baker, C.A., Blackledge, B., Goldsworth, F.W., Kennedy-Asser, A.T.,
577 Liu, Q., Sieradzan, K.R., Vosper, E., Ying, R.: The biological carbon pump
578 in CMIP6 models: 21st century trends and uncertainties. Proceedings of the
579 National Academy of Sciences **119**(29), 2204369119 (2022) <https://doi.org/10.1073/pnas.2204369119> . Publisher: Proceedings of the National Academy of
580 Sciences. Accessed 2023-11-08
- 581 [25] Dunne, J.P.: Physical Mechanisms Driving Enhanced Carbon Sequestration by
582 the Biological Pump Under Climate Warming. Global Biogeochemical Cycles
583 **37**(11), 2023-007859 (2023) <https://doi.org/10.1029/2023GB007859> . eprint:
584 <https://onlinelibrary.wiley.com/doi/pdf/10.1029/2023GB007859>. Accessed 2025-
585 04-11
- 586 [26] McGillicuddy, D.J., Anderson, L.A., Bates, N.R., Bibby, T., Buesseler, K.O.,
587 Carlson, C.A., Davis, C.S., Ewart, C., Falkowski, P.G., Goldthwait, S.A., Hansell,
588 D.A., Jenkins, W.J., Johnson, R., Kosnyrev, V.K., Ledwell, J.R., Li, Q.P., Siegel,
589 D.A., Steinberg, D.K.: Eddy/Wind Interactions Stimulate Extraordinary Mid-
590 Ocean Plankton Blooms. Science **316**(5827), 1021–1026 (2007) <https://doi.org/10.1126/science.1136256> . Publisher: American Association for the Advancement
591 of Science. Accessed 2023-04-21
- 592 [27] Chelton, D.B., Gaube, P., Schlax, M.G., Early, J.J., Samelson, R.M.: The Influ-
593 ence of Nonlinear Mesoscale Eddies on Near-Surface Oceanic Chlorophyll. Science
594 **334**(6054), 328–332 (2011) <https://doi.org/10.1126/science.1208897> . Publisher:
595 American Association for the Advancement of Science. Accessed 2025-04-11
- 596 [28] Claustre, H., Legendre, L., Boyd, P.W., Levy, M.: The Oceans' Biological Carbon
597 Pumps: Framework for a Research Observational Community Approach. Frontiers
598 in Marine Science **8** (2021). Accessed 2022-02-17
- 599 [29] Llort, J., Langlais, C., Matear, R., Moreau, S., Lenton, A., Strut-
600 ton, P.G.: Evaluating Southern Ocean Carbon Eddy-Pump From
601 Biogeochemical-Argo Floats. Journal of Geophysical Research: Oceans
602 **123**(2), 971–984 (2018) <https://doi.org/10.1002/2017JC012861> . eprint:
603 <https://onlinelibrary.wiley.com/doi/pdf/10.1002/2017JC012861>. Accessed
604 2022-01-31
- 605 [30] Lacour, L., Llort, J., Briggs, N., Strutton, P.G., Boyd, P.W.: Seasonality of
606

- downward carbon export in the Pacific Southern Ocean revealed by multi-year robotic observations. *Nature Communications* **14**(1), 1278 (2023) <https://doi.org/10.1038/s41467-023-36954-7>. Number: 1 Publisher: Nature Publishing Group. Accessed 2023-12-15
- [31] Stukel, M.R., Irving, J.P., Kelly, T.B., Ohman, M.D., Fender, C.K., Yingling, N.: Carbon sequestration by multiple biological pump pathways in a coastal upwelling biome. *Nature Communications* **14**(1), 2024 (2023) <https://doi.org/10.1038/s41467-023-37771-8>. Number: 1 Publisher: Nature Publishing Group. Accessed 2023-04-25
- [32] Baumas, C., Bizic, M.: A focus on different types of organic matter particles and their significance in the open ocean carbon cycle. *Progress in Oceanography* **224**, 103233 (2024) <https://doi.org/10.1016/j.pocean.2024.103233>. Accessed 2025-11-28
- [33] Archibald, K.M., Siegel, D.A., Doney, S.C.: Modeling the Impact of Zooplankton Diel Vertical Migration on the Carbon Export Flux of the Biological Pump. *Global Biogeochemical Cycles* **33**(2), 181–199 (2019) <https://doi.org/10.1029/2018GB005983>. eprint: <https://onlinelibrary.wiley.com/doi/pdf/10.1029/2018GB005983>. Accessed 2022-08-01
- [34] Estapa, M.L., Feen, M.L., Breves, E.: Direct Observations of Biological Carbon Export From Profiling Floats in the Subtropical North Atlantic. *Global Biogeochemical Cycles* **33**(3), 282–300 (2019) <https://doi.org/10.1029/2018GB006098>. eprint: <https://onlinelibrary.wiley.com/doi/pdf/10.1029/2018GB006098>. Accessed 2025-04-11
- [35] Haëntjens, N., Della Penna, A., Briggs, N., Karp-Boss, L., Gaube, P., Claustre, H., Boss, E.: Detecting Mesopelagic Organisms Using Biogeochemical-Argo Floats. *Geophysical Research Letters* **47**(6), 2019–086088 (2020) <https://doi.org/10.1029/2019GL086088>. eprint: <https://onlinelibrary.wiley.com/doi/pdf/10.1029/2019GL086088>. Accessed 2024-08-19
- [36] Lacour, L., Briggs, N., Claustre, H., Ardyna, M., Dall'Olmo, G.: The Intraseasonal Dynamics of the Mixed Layer Pump in the Subpolar North Atlantic Ocean: A Biogeochemical-Argo Float Approach. *Global Biogeochemical Cycles* **33**(3), 266–281 (2019) <https://doi.org/10.1029/2018GB005997>. eprint: <https://onlinelibrary.wiley.com/doi/pdf/10.1029/2018GB005997>. Accessed 2025-04-11
- [37] Lacour, L., Llort, J., Briggs, N., Strutton, P., Boyd, P.: Multi-year robotic observations reveal the seasonality of downward carbon export pathways in the Southern Ocean. Technical report (January 2022). <https://doi.org/10.21203/rs.3.rs-1006941/v1>. ISSN: 2693-5015 Type: article. <https://www.researchsquare.com/>

648 [article/rs-1006941/v1](https://doi.org/10.1029/2012GL052756) Accessed 2022-01-31

- 649 [38] Lévy, M., Ferrari, R., Franks, P.J.S., Martin, A.P., Rivière, P.:
650 Bringing physics to life at the submesoscale. *Geophysical Research
651 Letters* **39**(14) (2012) <https://doi.org/10.1029/2012GL052756> . eprint:
652 <https://onlinelibrary.wiley.com/doi/pdf/10.1029/2012GL052756>. Accessed
653 2022-08-22
- 654 [39] Poupon, M.A., Resplandy, L., Garwood, J., Stock, C., Zadeh, N., Luo, J.Y.:
655 Chlorophyll shading reduces zooplankton diel migration depth in a high-resolution
656 physical–biogeochemical model. *Ocean Science* **21**(2), 851–875 (2025) [https://doi.org/10.5194/os-21-851-2025](https://doi.
657 org/10.5194/os-21-851-2025) . Publisher: Copernicus GmbH. Accessed 2025-05-12
- 658 [40] Henson, S., Le Moigne, F., Giering, S.: Drivers of Carbon Export
659 Efficiency in the Global Ocean. *Global Biogeochemical Cycles* **33**(7),
660 891–903 (2019) <https://doi.org/10.1029/2018GB006158> . eprint:
661 <https://onlinelibrary.wiley.com/doi/pdf/10.1029/2018GB006158>. Accessed
662 2025-04-11
- 663 [41] Johnson, A.R., Omand, M.M.: Evolution of a Subducted Carbon-Rich Filament
664 on the Edge of the North Atlantic Gyre. *Journal of Geophysical Research: Oceans*
665 **126**(2), 2020–016685 (2021) <https://doi.org/10.1029/2020JC016685> . eprint:
666 <https://onlinelibrary.wiley.com/doi/pdf/10.1029/2020JC016685>. Accessed 2023-
667 10-30
- 668 [42] Ricour, F., Guidi, L., Gehlen, M., DeVries, T., Legendre, L.: Century-scale carbon
669 sequestration flux throughout the ocean by the biological pump. *Nature Geo-
670 science* **16**(12), 1105–1113 (2023) <https://doi.org/10.1038/s41561-023-01318-9> .
671 Publisher: Nature Publishing Group. Accessed 2024-09-14
- 672 [43] Irigoien, X.: Gut clearance rate constant, temperature and initial gut contents:
673 a review. *Journal of Plankton Research* **20**(5), 997–1003 (1998) [https://doi.org/10.1093/plankt/20.5.997](https://doi.org/
674 10.1093/plankt/20.5.997) . Accessed 2024-04-01
- 675 [44] Countryman, C.E., Steinberg, D.K., Burd, A.B.: Modelling the effects of copepod
676 diel vertical migration and community structure on ocean carbon flux using an
677 agent-based model. *Ecological Modelling* **470**, 110003 (2022) [https://doi.org/10.1016/j.ecolmodel.2022.110003](https://doi.org/10.
678 1016/j.ecolmodel.2022.110003) . Accessed 2025-04-11
- 679 [45] Thibault, H., Ménard, F., Abitbol-Spangaro, J., Poggiale, J.-C., Martini, S.:
680 Modeling the contribution of micronekton diel vertical migrations to carbon
681 export in the mesopelagic zone. *EGUphere*, 1–30 (2024) [https://doi.org/10.5194/egusphere-2024-2074](https://doi.org/10.5194/
682 egusphere-2024-2074) . Publisher: Copernicus GmbH. Accessed 2025-04-11
- 683 [46] Bonelli, A.G., Loisel, H., Jorge, D.S.F., Mangin, A., d'Andon, O.F., Vantrepotte,
684 V.: A new method to estimate the dissolved organic carbon concentration from
685 remote sensing in the global open ocean. *Remote Sensing of Environment* **281**,

- 686 113227 (2022) <https://doi.org/10.1016/j.rse.2022.113227> . Accessed 2025-11-30
- 687 [47] Huang, Y., Fassbender, A.J., Long, J.S., Johannessen, S., Bernardi Bif, M.: Partitioning the Export of Distinct Biogenic Carbon Pools in the Northeast Pacific
688 Ocean Using a Biogeochemical Profiling Float. *Global Biogeochemical Cycles*
689 **36**(2), 2021–007178 (2022) <https://doi.org/10.1029/2021GB007178> . eprint:
690 <https://agupubs.onlinelibrary.wiley.com/doi/pdf/10.1029/2021GB007178>. Accessed 2025-
691 11-30
- 692
- 693 [48] Zhang, Z., Miao, M., Qiu, B., Tian, J., Jing, Z., Chen, G., Chen,
694 Z., Zhao, W.: Submesoscale Eddies Detected by SWOT and Moored
695 Observations in the Northwestern Pacific. *Geophysical Research Letters*
696 **51**(15), 2024–110000 (2024) <https://doi.org/10.1029/2024GL110000> . eprint:
697 <https://onlinelibrary.wiley.com/doi/pdf/10.1029/2024GL110000>. Accessed 2025-
698 01-13
- 699 [49] Zakem, E.J., Cael, B.B., Levine, N.M.: A unified theory for organic matter accu-
700 cumulation. *Proceedings of the National Academy of Sciences* **118**(6), 2016896118
701 (2021) <https://doi.org/10.1073/pnas.2016896118> . Publisher: Proceedings of the
702 National Academy of Sciences. Accessed 2023-04-20
- 703 [50] Nguyen, T.T.H., Zakem, E.J., Ebrahimi, A., Schwartzman, J., Caglar, T., Amar-
704 nath, K., Alcolombri, U., Peaudecerf, F.J., Hwa, T., Stocker, R., Cordero, O.X.,
705 Levine, N.M.: Microbes contribute to setting the ocean carbon flux by altering
706 the fate of sinking particulates. *Nature Communications* **13**(1), 1657 (2022) <https://doi.org/10.1038/s41467-022-29297-2> . Number: 1 Publisher: Nature Publishing
707 Group. Accessed 2023-04-21
- 708
- 709 [51] Jiao, N., Herndl, G.J., Hansell, D.A., Benner, R., Kattner, G., Wilhelm, S.W.,
710 Kirchman, D.L., Weinbauer, M.G., Luo, T., Chen, F., Azam, F.: The micro-
711 bial carbon pump and the oceanic recalcitrant dissolved organic matter pool.
712 *Nature Reviews Microbiology* **9**(7), 555–555 (2011) <https://doi.org/10.1038/nrmicro2386-c5> . Publisher: Nature Publishing Group. Accessed 2024-11-06
- 713
- 714 [52] Jiao, N., Luo, T., Chen, Q., Zhao, Z., Xiao, X., Liu, J., Jian, Z., Xie, S., Thomas,
715 H., Herndl, G.J., Benner, R., Gonsior, M., Chen, F., Cai, W.-J., Robinson, C.: The microbial carbon pump and climate change. *Nature Reviews Microbiology*
716 **22**(7), 408–419 (2024) <https://doi.org/10.1038/s41579-024-01018-0> . Publisher:
717 Nature Publishing Group. Accessed 2025-04-11
- 718
- 719 [53] Luo, J.Y., Condon, R.H., Stock, C.A., Duarte, C.M., Lucas, C.H., Pitt,
720 K.A., Cowen, R.K.: Gelatinous Zooplankton-Mediated Carbon Flows in the
721 Global Oceans: A Data-Driven Modeling Study. *Global Biogeochemical Cycles*
722 **34**(9), 2020–006704 (2020) <https://doi.org/10.1029/2020GB006704> . eprint:
723 <https://agupubs.onlinelibrary.wiley.com/doi/pdf/10.1029/2020GB006704>. Accessed 2025-11-30
- 724

- 725 [54] Luo, J.Y., Stock, C.A., Henschke, N., Dunne, J.P., O'Brien, T.D.: Global ecological
726 and biogeochemical impacts of pelagic tunicates. *Progress in Oceanography*
727 **205**, 102822 (2022) <https://doi.org/10.1016/j.pocean.2022.102822> . Accessed
728 2025-11-30
- 729 [55] Clements, D.J., Stamieszkin, K., Bianchi, D., Blanco-Bercial, L., Record, N.R., Rodriguez-Perez, R.B., Maas, A.E.: Active Carbon Transport by Diel
730 Vertical Migrating Zooplankton: Calculated and Modeled, but Never Measured
731 (2025) <https://doi.org/10.1146/annurev-marine-121422-015330> . Publisher:
732 Annual Reviews. Accessed 2025-09-15
- 733 [56] Maas, A.E., Timmins-Schiffman, E., Tarrant, A.M., Nunn, B.L., Park, J., Blanco-Bercial, L.: Diel metabolic patterns revealed by in situ transcriptome and proteome in a vertically migratory copepod. *Molecular Ecology* **33**(6), 17284 (2024) <https://doi.org/10.1111/mec.17284> . eprint:
734 <https://onlinelibrary.wiley.com/doi/pdf/10.1111/mec.17284>. Accessed 2025-01-
735 16
- 736 [57] Séférian, R., Berthet, S., Yool, A., Palmiéri, J., Bopp, L., Tagliabue, A.,
737 Kwiatkowski, L., Aumont, O., Christian, J., Dunne, J., Gehlen, M., Ilyina,
738 T., John, J.G., Li, H., Long, M.C., Luo, J.Y., Nakano, H., Romanou, A.,
739 Schwinger, J., Stock, C., Santana-Falcón, Y., Takano, Y., Tjiputra, J., Tsujino,
740 H., Watanabe, M., Wu, T., Wu, F., Yamamoto, A.: Tracking Improvement in Sim-
741ulated Marine Biogeochemistry Between CMIP5 and CMIP6. *Current Climate
742 Change Reports* **6**(3), 95–119 (2020) <https://doi.org/10.1007/s40641-020-00160-0>
743 . Accessed 2024-07-17
- 744 [58] Henson, S., Baker, C.A., Halloran, P., McQuatters-Gollop, A., Painter, S., Plan-
745 chat, A., Tagliabue, A.: Knowledge Gaps in Quantifying the Climate Change
746 Response of Biological Storage of Carbon in the Ocean. *Earth's Future* **12**(6),
747 2023–004375 (2024) <https://doi.org/10.1029/2023EF004375> . Accessed 2025-12-
748 11
- 749 [59] Wang, B., Fennel, K.: Distinct sources of uncertainty in simulations of the ocean
750 biological carbon pump at different depths. *Communications Earth & Environ-
751 ment* **5**(1), 395 (2024) <https://doi.org/10.1038/s43247-024-01561-x> . Publisher:
752 Nature Publishing Group. Accessed 2025-12-11
- 753 [60] Martin, A.P., Dominguez, A.B., Baker, C.A., Baumas, C.M.J., Bisson, K.M.,
754 Cavan, E., Freilich, M., Galbraith, E., Galí, M., Henson, S., Kvale, K.F., Lem-
755 men, C., Luo, J.Y., McMonagle, H., Viríssimo, F.d.M., Möller, K.O., Richon, C.,
756 Suresh, I., Wilson, J.D., Woodstock, M.S., Yool, A.: When to add a new pro-
757 cess to a model – and when not: A marine biogeochemical perspective. *Ecological
758 Modelling* **498**, 110870 (2024) <https://doi.org/10.1016/j.ecolmodel.2024.110870> .
759 Accessed 2024-09-30
- 760 [61] Baltar, F., Arístegui, J., Sintes, E., Gasol, J.M., Reinthaler, T., Herndl, G.J.:
761

- 765 Significance of non-sinking particulate organic carbon and dark CO₂ fixation to
766 heterotrophic carbon demand in the mesopelagic northeast Atlantic. Geophysical
767 Research Letters **37**(9) (2010) <https://doi.org/10.1029/2010GL043105> . eprint:
768 <https://agupubs.onlinelibrary.wiley.com/doi/pdf/10.1029/2010GL043105>. Accessed 2025-11-28
- 770 [62] Reinthalter, T., Aken, H.M., Herndl, G.J.: Major contribution of autotrophy to
771 microbial carbon cycling in the deep North Atlantic's interior. Deep Sea Research
772 Part II: Topical Studies in Oceanography **57**(16), 1572–1580 (2010) <https://doi.org/10.1016/j.dsr2.2010.02.023> . Accessed 2025-11-28
- 774 [63] Adcroft, A., Anderson, W., Balaji, V., Blanton, C., Bushuk, M., Dufour,
775 C.O., Dunne, J.P., Griffies, S.M., Hallberg, R., Harrison, M.J., Held, I.M.,
776 Jansen, M.F., John, J.G., Krasting, J.P., Langenhorst, A.R., Legg, S., Liang,
777 Z., McHugh, C., Radhakrishnan, A., Reichl, B.G., Rosati, T., Samuels, B.L.,
778 Shao, A., Stouffer, R., Winton, M., Wittenberg, A.T., Xiang, B., Zadeh,
779 N., Zhang, R.: The GFDL Global Ocean and Sea Ice Model OM4.0: Model
780 Description and Simulation Features. Journal of Advances in Modeling Earth
781 Systems **11**(10), 3167–3211 (2019) <https://doi.org/10.1029/2019MS001726> . eprint:
782 <https://onlinelibrary.wiley.com/doi/pdf/10.1029/2019MS001726>. Accessed 2022-
783 10-16
- 784 [64] Stock, C.A., Dunne, J.P., Fan, S., Ginoux, P., John, J., Krasting,
785 J.P., Laufkötter, C., Paulot, F., Zadeh, N.: Ocean Biogeochemistry in
786 GFDL's Earth System Model 4.1 and Its Response to Increasing Atmo-
787 spheric CO₂. Journal of Advances in Modeling Earth Systems **12**(10),
788 2019-002043 (2020) <https://doi.org/10.1029/2019MS002043> . eprint:
789 <https://onlinelibrary.wiley.com/doi/pdf/10.1029/2019MS002043>. Accessed
790 2022-10-16
- 791 [65] Stock, C.A., Dunne, J.P., John, J.G.: Global-scale carbon and energy flows
792 through the marine planktonic food web: An analysis with a coupled physi-
793 cal–biological model. Progress in Oceanography **120**, 1–28 (2014) <https://doi.org/10.1016/j.pocean.2013.07.001> . Accessed 2023-05-18
- 795 [66] Laufkötter, C., John, J.G., Stock, C.A., Dunne, J.P.: Temperature and oxygen
796 dependence of the remineralization of organic matter. Global Biogeochemical
797 Cycles **31**(7), 1038–1050 (2017) <https://doi.org/10.1002/2017GB005643> . eprint:
798 <https://agupubs.onlinelibrary.wiley.com/doi/pdf/10.1002/2017GB005643>. Accessed 2025-11-28
- 800 [67] De Boyer Montégut, C.: Mixed layer depth climatology computed with a
801 density threshold criterion of 0.03kg/m³ from 10 m depth value. SEANOE
802 (2023). <https://doi.org/10.17882/91774> . <https://www.seanoe.org/data/00806/91774/> Accessed 2024-12-03
- 804 [68] Behrenfeld, M.J., Gaube, P., Della Penna, A., O'Malley, R.T., Burt, W.J., Hu,

- 805 Y., Bontempi, P.S., Steinberg, D.K., Boss, E.S., Siegel, D.A., Hostetler, C.A.,
 806 Tortell, P.D., Doney, S.C.: Global satellite-observed daily vertical migrations
 807 of ocean animals. *Nature* **576**(7786), 257–261 (2019) <https://doi.org/10.1038/s41586-019-1796-9>. Number: 7786 Publisher: Nature Publishing Group. Accessed
 808 2022-07-27
- 810 [69] Steinberg, D.K., Lomas, M.W., Cope, J.S.: Long-term increase in meso-
 811 zooplankton biomass in the Sargasso Sea: Linkage to climate and impli-
 812 cations for food web dynamics and biogeochemical cycling. *Global Bioge-
 813 ochemical Cycles* **26**(1) (2012) <https://doi.org/10.1029/2010GB004026> . _eprint:
 814 <https://onlinelibrary.wiley.com/doi/pdf/10.1029/2010GB004026>. Accessed 2023-
 815 12-06
- 816 [70] Behrenfeld, M.J., Falkowski, P.G.: A consumer's guide to phytoplankton primary
 817 productivity models. *Limnology and Oceanography* **42**(7), 1479–1491 (1997)
 818 <https://doi.org/10.4319/lo.1997.42.7.1479> . Accessed 2024-06-19
- 819 [71] Westberry, T., Behrenfeld, M.J., Siegel, D.A., Boss, E.: Carbon-based pri-
 820 mary productivity modeling with vertically resolved photoacclimation. *Global*
 821 *Biogeochemical Cycles* **22**(2), 2007–003078 (2008) <https://doi.org/10.1029/2007GB003078> . Accessed 2024-06-19
- 823 [72] Silsbe, G.M., Behrenfeld, M.J., Halsey, K.H., Milligan, A.J., Westberry, T.K.:
 824 The CAFE model: A net production model for global ocean phytoplankton.
 825 *Global Biogeochemical Cycles* **30**(12), 1756–1777 (2016) <https://doi.org/10.1002/2016GB005521> . Accessed 2024-06-19
- 827 [73] Dall'Olmo, G., Bhaskar TVS, U., Bittig, H., Boss, E., Brewster, J., Claustre, H.,
 828 Donnelly, M., Maurer, T., Nicholson, D., Paba, V., Plant, J., Poteau, A., Sauzède,
 829 R., Schallenberg, C., Schmechtig, C., Schmid, C., Xing, X.: Real-time quality
 830 control of optical backscattering data from Biogeochemical-Argo floats. *Open*
 831 *Research Europe* **2**, 118 (2023) <https://doi.org/10.12688/openreseurope.15047.2> . Accessed 2024-08-19
- 833 [74] Lauvset, S.K., Lange, N., Tanhua, T., Bittig, H.C., Olsen, A., Kozyr, A., Álvarez,
 834 M., Azetsu-Scott, K., Brown, P.J., Carter, B.R., Cunha, L., Hoppema, M.,
 835 Humphreys, M.P., Ishii, M., Jeansson, E., Murata, A., Müller, J.D., Pérez, F.F.,
 836 Schirnick, C., Steinfeldt, R., Suzuki, T., Ulfsbo, A., Velo, A., Woosley, R.J., Key,
 837 R.M.: The annual update GLODAPv2.2023: the global interior ocean biogeo-
 838 chemical data product. *Earth System Science Data* **16**(4), 2047–2072 (2024) <https://doi.org/10.5194/essd-16-2047-2024> . Publisher: Copernicus GmbH. Accessed
 839 2025-04-11
- 841 [75] Hansell, D.A., Carlson, C.A., Amon, R.M.W., Álvarez-Salgado, X.A., Yamashita,
 842 Y., Romera-Castillo, C., Bif, M.B.: Compilation of dissolved organic matter
 843 (DOM) data obtained from global ocean observations from 1994 to 2021. Version 2

- 844 (NCEI Accession 0227166). NOAA National Centers for Environmental Information
845 (2021). <https://doi.org/10.25921/S4F4-YE35> . <https://www.ncei.noaa.gov/archive/accession/0227166> Accessed 2024-12-03
- 846
- 847 [76] Buesseler, K.O., Boyd, P.W., Black, E.E., Siegel, D.A.: Metrics that matter for
848 assessing the ocean biological carbon pump. Proceedings of the National Academy
849 of Sciences **117**(18), 9679–9687 (2020) <https://doi.org/10.1073/pnas.1918114117>.
850 Publisher: Proceedings of the National Academy of Sciences. Accessed 2023-10-13
- 851 [77] Levy, M., Couespel, D., Haeck, C., Keerthi, M.G., Mangolte, I., Prend, C.J.:
852 Impact of finescale currents on biogeochemical cycles in a changing ocean. Annual
853 Review of Marine Science (2023) [https://doi.org/10.1146/\(\(please](https://doi.org/10.1146/((please) . Accessed
854 2023-04-20
- 855 [78] Bianchi, D., Mislan, K.a.S.: Global patterns of diel vertical migra-
856 tion times and velocities from acoustic data. Limnology and Oceanog-
857 raphy **61**(1), 353–364 (2016) <https://doi.org/10.1002/lno.10219> . eprint:
858 <https://onlinelibrary.wiley.com/doi/pdf/10.1002/lno.10219>. Accessed 2023-04-20